Comparison of Relative Permeability-Saturation-Capillary Pressure Models for Simulation of Reservoir CO_2 Injection

M. Oostrom[*1], M.D. White[1], S.C.M. Krevor[2], and S.A. Mathias[3]

Submitted to *International Journal of Greenhouse Gas Control*
August 2015

---

* Corresponding Author
[1]Energy and Environment Division, Pacific Northwest National Laboratory,
P.O. Box 999, MS K9-33,
Richland, WA 99354
USA
[2]Dept. of Earth Science and Engineering, Imperial College London, UK
[3]Dept. of Earth Sciences, Durham University, Durham, UK

Abstract

Constitutive relations between relative permeability (k_r), fluid saturation (S), and capillary pressure (P_c) determine to a large extent the distribution of brine and supercritical CO_2 ($scCO_2$) during subsurface injection operations. Published numerical multiphase simulations for brine- $scCO_2$ systems so far have primarily used four $k_r - S - P_c$ models. For the $S - P_c$ relations, either the Brooks-Corey (BC) or Van Genuchten (VG) equations are used. The $k_r - S$ relations are based on the Mualem, Burdine, or Corey equations without the consideration of experimental data. Recently, two additional models have been proposed where the $k_r - S$ relations are obtained by fitting to experimental data using either an endpoint power law or a modified Corey approach. The six models were tested using data from four well-characterized sandstones (Berea, Paaratte, Tuscaloosa, Mt. Simon) for two radial injection test cases. The results show a large variation in plume extent and saturation distribution for each of the sandstones, depending on the used model. The VG-Mualem model predicts plumes that are considerably larger than for the other models due to the overestimation of the gas relative permeability. On the other hand, the predicted plume sizes are the smallest for the VG-Corey model due to the underestimation of the aqueous phase relative permeability. Of the four models that do not use fits to experimental relative permeability data, the hybrid model with Mualem aqueous phase and Corey gas phase relative permeabilities provide the best fits to the experimental data and produce results close to the model with fits to the capillary pressure and relative permeability data. The model with the endpoint power law resulted in very low, uniform gas saturations outside the dry-out zone for the Tuscaloosa sandstone, as the result of a rapidly declining aqueous

phase relative permeability. This observed behavior illustrates the need to obtain reliable relative permeability relations for a potential reservoir, beyond permeability and porosity data.

Nomenclature

α: van Genuchten parameter, 1/Pa

k_{rj}: phase *j* relative permeability

k_{rj0}: phase *j* endpoint relative permeability

λ: Brooks-Corey pore geometry factor

n_v: van Genuchten shape parameter

m_v: $(=1-1/n_v)$ van Genuchten shape parameter

N_{j-vC}: coefficient for variable Corey relative permeability model (phase *j)*

N_{j-EPL}: coefficient for endpoint power law relative permeability model (phase *j*)

P_c: capillary pressure, Pa

P_e: Brooks-Corey entry pressure, Pa

P_o: $(=1/\alpha)$ strength coefficient, Pa

S_j: phase *j* actual saturation

$\bar{S}_j$: phase *j* effective saturation

S_{li}: aqueous phase irreducible saturation

S_{l0}: aqueous phase endpoint saturation

subscripts:

g: gas phase

l: aqueous phase

1. Introduction

The option of carbon sequestration in deep formations (e.g., coalbeds, saline aquifers, and oil and gas reservoirs) is developing rapidly as a promising method to mitigate the adverse impacts of climate change. Of the deep formations, saline aquifers, widely distributed around the globe in sedimentary basins, offer the largest storage potential. Numerical simulation of the injection and redistribution of supercritical CO_2 ($scCO_2$) is important to determine storage capacity, formation pressure, plume extent and shape, and leakage potential. Ideally, numerical simulators should have the ability to represent the four primary mechanisms identified for CO_2 trapping (Doughty, 2010): stratigraphic or structural, residual, dissolution, and mineral. Given that mineral trapping typically occurs over very long time scales (Pruess et al., 2003), the first three mechanisms, often referred to as hydrodynamic trapping, dominate plume behavior during injection and immediately thereafter over a hundred-year time scale (Doughty, 2010). Given the dominance of the stratigraphic, residual, and dissolution trapping mechanism in the near future, most major simulators with capabilities for CO_2 storage (e.g., TOUGH2 (Pruess et al., 1999; Pruess and Spycher, 2007) and STOMP (White and Oostrom, 2006; White et al., 2010)) focus on these processes.

In these simulators, interaction between the reservoir brine (wetting phase) and $scCO_2$ (nonwetting phase) occurs through constitutive relations between relative permeability (k_r), fluid saturation (S), and capillary pressure (P_c). In reservoir simulators like Eclipse (Schlumberger, 2010) capillary flow at the grid block scale is often considered to negligible and only $k_r - S$ relations are specified (Benisch et al., 2013; Chadwick et al., 2012; Pham et al., 2013). For the simulators

requiring both $k_r - S$ and $S - P_c$ relations as inputs, it has been established that these constitutive relations determine to a large extent the plume shape and phase distribution (Class et al., 2009; Juanes, 2006; Pruess and Garcia, 2002).

Simulation of hydrodynamic trapping and pore-geometry hysteresis typically requires the consideration of $k_r - S$ and $S - P_c$ hysteresis as these relations are functions of saturation history and the displacement process (drainage or imbibition). However, full hysteretic formulations, including both fluid entrapment and pore geometry hysteresis, are complex and may result in considerable computational demands. Due to the complexity of incorporating hysteresis, models that provide a full hysteretic capability are limited. An exception is the work by Doughty (2007; 2010) who described the implementation of a hysteric model in TOUGH2. Alternatively, simpler models allowing gas entrapment as the only hysteretic mechanism in $S - P_c$ (Krevor et al., 2012; White et al., 2013) or $k_r - S$ relations (Pham et al., 2013; Senel et al., 2015) are more widespread. As stated by Doughty (2007), the use of hysteretic constitutive relations is not important for the simulation of the CO_2 injection stage because the plume is continuously growing and all locations follow the primary drainage branch of the $S - P_c$ curves, which can be replicated using a non-hysteretic formulation. In the analysis presented in this paper, only displacement processes during injection are considered, allowing for the comparison of nonhysteretic constitutive relations.

The parameter values for the $k_r - S$ and $S - P_c$ relations are typically obtained for comparable formations from data in the literature (Schnaar and Digiulio, 2009). Alternatively, these values can be obtained by fitting the relations to experimentally obtained datasets. For the $S - P_c$ relations, a common and inexpensive experimental procedure is the mercury injection capillary pressure

(MICP) method, using small rock samples. Due to the sample size and potential issues related to the translation of the mercury data into $scCO_2$-brine fluid pair $S - P_c$ relations, the applicability of the method is not without controversy. Pini et al. (2012) derived $S - P_c$ relationships with $scCO_2$-brine systems at reservoir conditions using a CT scanner. While the technique used is perhaps too costly and time-consuming for widespread application, it demonstrated the validity of using capillary pressure curves derived from MICP or other analogue water-wet fluid systems. For the $k_r - S$ relations, an inexpensive experimental method (Muller, 2011) does not exist and uncertainty persists around the best measurement techniques and the quality of existing $scCO_2$-brine $k_r - S$ data sets (Benson et al., 2015). Modelers therefore tend to use relations that minimize the use of fitted parameter values or use relations based on the scarce data sets (e.g., Bachu and Bennion, 2010; Bennion and Bachu, 2008, 2010). Recently, CT scanners were used by Akbarabadi and Piri (2013), Krevor et al. (2012), Ruprecht et al., (2014) and Perrin and Benson (2010) to obtain high-quality $k_r - S$ data sets. The increased understanding of the appropriate measurement techniques for CO_2 relative permeability suggests there is potential to expand the availability of $k_r - S$ data sets in the near future (Benson et al., 2013, 2015).

The two major $S - P_c$ models used for nonhysteretic subsurface $scCO_2$ injection simulations are based on retention relations proposed by van Genuchten (1980) and Brooks-Corey (1964) and are listed in Table 1. In the Van Genuchten (VG) model, α (Pa^{-1}) is roughly the inverse of the gas entry pressure, and n_v and m_v are pore-geometry parameters related by $m_v = 1 - 1/n_v$. A main characteristic of the VG $S - P_c$ relation is that the wetting fluid is displaced by the nonwetting fluid if $P_c > 0$. Based on the assumption that $P_e \approx 1/\alpha$ (Pa), $1/\alpha$ is often represented in the VG $S - P_c$ equation by the strength coefficient P_o (e.g.,

Birkholzer et al, 2009; Doughty, 2010; Mathias et al., 2013; Yamamoto et al., 2009). It is important to realize that although a finite pressure P_o is part of the alternative VG equation (Table 1), P_o does not constitute an entry pressure: The porous medium still desaturates with respect to the wetting fluid when $P_c > 0$ (Lenhard et al., 1989). For the Brooks-Corey (BC) $S - P_c$ relation, values of a $P_e > 0$ and a pore-geometry parameter λ are prescribed (Table 1). Both the VG and BC models are easily fitted to experimental retention data and the parameterization of either one of the relations can be used to find the corresponding other relation by using a method developed by Lenhard et al. (1989).

Most $k_r - S$ relations reported in the subsurface scCO2 literature use the empirical model proposed by Corey (1964) or the geometry-based models of Burdine (1953) and Mualem (1978). Corey's (1964) simple polynomial functions have been widely used in the petroleum literature. The two geometry-based models relate relative permeability to the $S - P_c$ curve based on the simple geometric assumption that the pore space is a bundle of capillary tubes (Dury et al., 1999). Both the Burdine (1953) and Mualem (1978) relative permeability models consist of the product of an empirical connectivity/tortuosity term and an integral term representing the actual capillary theoretical model. Assuming that in a water-wet porous medium the nonwetting fluid is residing in the largest pores, the relative permeabilities for both models can be written as

$$k_{rl} = \bar{S}_l^{\,a} \left[\frac{\int_0^{\bar{S}_l} \frac{dx}{h^b(x)}}{\int_0^1 \frac{dx}{h^b(x)}} \right]^c \qquad (1a)$$

$$k_{rg} = \left(1 - \bar{S}_l\right)^a \left[\frac{\int_{\bar{S}_l}^{1} \frac{dx}{h^b(x)}}{\int_{0}^{1} \frac{dx}{h^b(x)}} \right]^c \tag{1b}$$

where x is a dummy integration value, and $h(\bar{S}_l)$ is the inverted $S - P_c$ relation. For the Burdine (1953) model, b = 2, and c = 1. For the Mualem (1978) model, b = 1, and c = 2. Mualem (1978) suggested a value of 0.5 for the tortuosity coefficient a, based on wetting fluid permeability data, whereas Burdine (1953) proposed an empirical value of 2. None of these values were based on theoretical considerations. When nonhysteretic $k_r - S$ relations are obtained according to Eq. (1), the resulting $k_r - S - P_c$ model is considered to be coupled through the m_v and λ parameters for the VG and BC relations, respectively. A discussion of the effects of coupling in constitutive relations is provided by DeHoff et al. (2011).

Although combining the VG and BC $S - P_c$ relations with either the Burdine (1953), Corey (1964), or Mualem (1978) $k_r - S$ relations could lead to a large number of $k_r - S - P_c$ models, just four of them are primarily used in the subsurface $scCO_2$ literature: the VG-Mualem (VG-M), BC-Burdine (BC-B), and VG-Corey (VG-C) models, and a model combining the VG $S - P_c$ relation with the Mualem relation for $k_{rl} - S$ and the Corey relation for $k_{rg} - S$. The latter model is referred to as the VG-hMC model where the h denotes that a hybrid Mualem-Corey $k_r - S$ model is used. It is noted that other $k_r - S$ relations have occasionally been used in the modeling literature but not at a level that warrants inclusion in this analysis. Examples of sparingly used models are cubic Corey-type expression for relative permeability (Vilarrasa, 2014), or linear interpolation between experimentally obtained relative permeability data points (Mtiku and Bauer, 2013).

Some of the reasons the empirical and geometry-based $k_r - S$ models have been widely used in subsurface scCO$_2$ modeling include the relative ease in implementation into numerical simulators and the lack of site-specific data, potentially masking the need to use more appropriate representations. As an alternative to these models, two promising $k_r - S$ models have been recently introduced that are obtained by fitting to experimental data. The VG-EPL model (Mathias et al., 2013) uses endpoint power law (EPL) equations and the BC-vC model (Krevor et al., 2012) uses Corey-type equations with variable exponents to obtain relative permeability relations. Although these two models are relatively recent, it is expected that the use of the proposed approaches will increase in the future when more site-specific data becomes available (Benson et al., 2013).

An overview of the $S - P_c$ and $k_r - S$ relations for the six considered models in this analysis (VG-M, BC-B, VG-C, VG-hMC, VG-EPL, and BC-vC) is presented in Table 1 and brief descriptions of each of the models are provided below. The VG-M model has been used by Birkholzer et al. (2009) to investigate pressure responses in stratified deep saline aquifers. Zhang and Agarwal (2013) used this model to simulate optimization of CO$_2$ sequestration but did not present any parameter values. Gor et al. (2013) did not provide parameter values in their VG-M simulations of thermal stresses on caprock integrity. It should be noted that only the $k_{rl} - S$ relation was formally derived by van Genuchten (1980) and that $k_{rg} - S$ relation was first presented by Lenhard and Parker (1987). Hysteretic VG-M models have been used by Doughty et al. (2008) and Doughty (2010) to predict plume behavior during and after injection at the Frio brine pilot in Texas and the Kimberlina site in California, respectively. The full hysteretic VG-M model, based on the model developed by Parker and Lenhard (1987) and Lenhard and Parker (1987) was presented in Doughty et al. (2007). The VG-M model is an

example of a coupled $k_r - S - P_c$ model if the same pore-geometry m_v parameter value is used in both the $S - P_c$ and $k_r - S$ relations. Coupling was used in Birkholzer et al. (2009), Doughty (2007) and Doughty et al. (2008). However, Doughty (2010) used different m_v values for the capillary pressure and relative permeability relations.

The BC-B model is also mostly used as a coupled $k_r - S - P_c$ model through the pore-geometry λ parameter. The BC-B model has been primarily used in benchmarking simulations (Class et al., 2009; Ebigbo et al., 2007; Kolditz et al., 2012) but also for an analysis coupled wellbore-reservoir flow during injection (Rasmussen et al., 2015). Interestingly, the λ value for the injection benchmark problems discussed by Kolditz et al. (2012) is omitted in their Table 4. Bandilla et al. (2012) mentioned the use of the BC-B model but did not report BC parameter values.

The VG-C model is an example of an uncoupled approach as the Corey (1954) $k_r - S$ relation is used where both phase relative permeabilities are only a function of the effective water saturation (Table 1) and is the same for all sediments. Examples of the model use are presented by Alkan et al. (2010), numerically investigating the combined effects of capillary pressure, salinity and in situ thermodynamic conditions on CO_2-brine-rock interactions in a saline aquifer, and by Kim et al. (2012), simulating salt precipitation and associated pressure build up.

The VG-hMC is by far the most widely used model for $scCO_2$ injection with contributions from, among others, Espinet et al. (2013), Giorgis et al. (2007), Liu et al. (2011), Middleton et al. (2012), Oldenburg et al. (2001), Okwen et al. (2011), Pruess and Muller (2009), Rutquist et al. (2007), Yamamoto and Doughty (2011), Yamamoto et al. (2009), Xu et al. (2007), and Zhou et al. (2010). The hybrid

approach uses the Mualem $k_{rl} - S$ function, typically coupled via the m_v parameter to the VG $S - P_c$ relation, and the uncoupled $k_{rg} - S$ Corey function. Exceptions are the simulations of Yamamoto and Doughty (2011) and Xu et al. (2010), who have used uncoupled Mualem $k_{rl} - S$ functions. Giorgis et al. (2007) did not list the parameter values for the conducted salt precipitation modeling. All of the listed VG-hMC references were completed with the TOUGH2-ECO2N simulator (Pruess et al. 1999; Pruess and Spycher, 2007). Of interest is the observation that for a large number of the VG-hMC papers, an m_v value of 0.457 was used as a generic parameter value (e.g., Espinet et al., 2013; Liu et al., 2011; Rutquist et al., 2007; Okwen et al., 2011; Xu et al., 2007; Yamamoto et al., 2009). This value was also used by Birkholzer et al. (2009) using the VG-M, and by Kim et al. (2012) using the VG-C relations. The origin of this ubiquitous value is not immediately clear, although Birkholzer et al. (2009) state that the value is typical for sedimentary formations suitable for CO_2 storage. Another widely used value for m_v in VG-hMC simulations is 0.412 (e.g., Middleton et al. 2012; Yamamoto and Dougthy, 2011; Zhou et al., 2010). This value was also used in the VG-M simulations reported by Doughty (2007; 2010) and Doughty et al. (2008) and originates from Sakurai et al. (2005).

The application of the VG-EPL model is explained in detail by Mathias et al. (2013). The endpoint power laws used in the model are common relations used in the petroleum literature (e.g., Orr, 2007). A complication in using the VG-EPL model is that the physical meaning of the endpoint S_{l0} in the relative permeability relations (i.e., the aqueous saturation at the largest experimentally obtained k_{rg}) is not necessarily the same as the irreducible saturation S_{li} in the VG $S - P_c$ equations (Table 1) because the values typically come from different

sources. However, if an EPL relative permeability model is used, the S_{li} in the associated VG relation has to be equal to S_{l0} so that $\bar{S}_l = (S_l - S_{l0})/(1 - S_{l0})$. The VG-EPL models reported in the literature (e.g., Mathias et al., 2013) typically employ a generic VG relation with P_e, n_v and m_v parameter values independent of the rock.

The other model using fitted $k_r - S$ relations, the BC-vC model, uses variable exponents, with values depending on the fit to the experimental data (Table 1). Krevor et al. (2012) proposed using this modified Corey (1954) approach to allow for the inclusion of fitted gas relative permeability values beyond the experimentally obtained gas saturation endpoint value. A major difference with the VG-EPL model is that the fitted S_{li} value in the $S - P_c$ model is also used in the $k_r - S$ relations. The BC-vC model has been used by Cameron and Durlovsky (2012).

So far, comparisons of the major $k_r - S - P_c$ models for subsurface $scCO_2$ behavior have been limited. Lu et al. (2009) compared numerical simulations using linear, cubic, VG-M, and interpolated $k_r - S$ relations to analytic sharp interface models. They concluded that the analytical models did not perform very well because due to the omission of capillary pressure and relative permeability data. Court et al. (2012) extended the analysis by Lu et al. (2009) to include comparisons with vertical equilibrium models. The authors found satisfactory agreement for a large range of $k_r - S$ relations, representing different rocks, as long as the equilibrium models are applied within the appropriate length and time scales. Both studies did not explicitly compare the performance of the used $k_r - S$ models.

The objective of this work is to compare the listed $k_r - S - P_c$ models in Table 1 for $scCO_2$ injection into four homogeneous sandstone reservoirs (Berea,

Paaratte, Tuscaloosa, and Mt. Simon). The parameter values for the models are obtained by fitting $S - P_c$ relations (for all models) and $k_r - S$ relations (for the VG-EPL and BC-vC models only) to experimental data provided by Krevor et al. (2012). For the models that use non-fitted $k_r - S$ relations, the used relations are based on empiricism or on capillary pressure data. Although the consensus is that it is vastly better to use models fully fitted to experimental data, it is not known what the performance is of models that only fit capillary pressure. The simulations are conducted for one-dimensional (1-D) and two-dimensional (2-D) configurations, described Mathias et al. (2013). In this comparison, only the main drainage process (aqueous phase displaced by $scCO_2$) in water-wet porous media is modeled and therefore no $scCO_2$ entrapment or pore-geometry hysteresis is considered.

2. Methods

Numerical Simulator

The $k_r - S - P_c$ model comparison has been conducted with STOMP-CO2, a fluid injection and production simulator for multiphase component flow and transport (White and Oostrom, 2006; White et al., 2010). The simulator has been verified against other simulation codes capable of modeling CO_2 flow and transport that were part of the GeoSeq code intercomparison study (Pruess and Garcia, 2002). For isothermal conditions without salt transport, as assumed in this contribution, mass conservation equations for water and CO_2 mass are solved. The conservation equations are converted to algebraic form using the finite volume approach applied to structured orthogonal grids and Euler-backwards time differencing. Each conservation equation is solved for a single unknown, such as fluid pressure, referred to as the primary variable. Because of

phase appearances and disappearances, four sets of primary variables are used depending on the phase condition. Constitutive relations, like the $k_r - S - P_c$ models, relate primary to secondary variables. Although the STOMP-CO2 simulator allows for hydraulic entrapment, the reported simulations describe constant CO_2 injection and, therefore, nonhysteretic $k_r - S - P_c$ relations were used. The CO_2 properties were developed from the CO_2 equations of state presented by Span and Wagner (1996).

To simulate formation dry-out, vapor pressure lowering according to Kelvin law's application to porous media (Nitao, 1988) is used in combination with extensions below irreducible aqueous phase saturation for the traditional van Genuchten (1980) and Brooks-Corey (1964) $S - P_c$ relations. The $S - P_c$ models are extended to allow for dry-out using the Webb (2000) procedure, resulting in the use of the existing relations above a computed saturation matching point, and a log-linear $S - P_c$ relation below this saturation, all the way to $S_l = 0$. A newly implemented phase condition allows for a primarily variable switch of the water conservation equation from water pressure to water vapor partial pressure when the aqueous saturation falls below the machine precision.

Sandstone Properties and $k_r - S - P_c$ Model Parameter Values

Simulations were conducted for constant-rate injections into four sandstone formations: Berea, Paaratte, Tuscaloosa, and Mt. Simon. The porosity and permeability were determined by Krevor et al. (2012) on rock cores and are listed in Table 2. The Berea and Paaratte rock cores were classified as high, the Tuscaloosa rock as moderate, and the Mt. Simon as low permeability sandstone. For all sandstones, a compressibility of 4.5×10^{-10} 1/Pa was assumed.

The $k_r - S - P_c$ parameter values for the six models are shown in Table 3 for

all four sandstones. The listed values are based on experimental $S - P_c$ and $k_r - S$ data presented by Krevor et al. (2012). The $S - P_c$ data were obtained using a standard mercury injection method, and were subsequently converted to brine – CO_2 systems assuming a brine-CO_2 interfacial tension of 32 mN/m and a contact angle of 40°. The $k_r - S$ data were obtained by performing a series of steady-state drainage experiments under reservoir conditions with *in situ* saturation monitoring using an X-ray CAT scanner (Krevor et al. 2012; Perrin and Benson 2010).

The listed $S - P_c$ parameter values in Table 3, associated with Brooks-Corey curve fits to the Berea, Paaratte, and Mt. Simon data, were obtained by Krevor et al. (2012), and are used in the BC-B and BC-vC models of this analysis (Table 1). As the shape of the Tuscaloosa $S - P_c$ data was somewhat irregular, Krevor et al. (2012) did not present parameter values for that rock. For this analysis, the Tuscaloosa entry pressure was computed with the Leverett-J function, using the Mt. Simon permeability and porosity (Table 1) as reference values. The choice of the Mt. Simon rock core as a reference rock is justified by recognizing, based on the data shown in Krevor et al. (2012), that the Tuscaloosa entry pressure is smaller than that of the other three rock cores, excluding the Berea and Paaratte as possible reference rock candidates.

The inverse of a procedure presented by Lenhard et al. (1989) has been used to obtain the equivalent van Genuchten curves from the Brooks-Corey relations, resulting in the parameter values shown in Table 3 for the VG-M, VG-C, and VG-hMC models. The only difference between the van Genuchten relation for the VG-EPL model and the van Genuchten $S - P_c$ relation used in the VG-M, VG-C, and VG-hMC models is the value of the irreducible aqueous phase saturation. For consistency with the EPL $k_r - S$ model, the endpoint aqueous phase

saturation, S_{l0}, is used as the irreducible aqueous phase saturation in each of the $S - P_c$ relations. This approach was applied by Mathias et al. (2013) in their relative permeability uncertainty analysis on CO_2 injectivity estimation.

The Brooks-Corey, the equivalent van Genuchten, and the van Genuchten curves for the EPL models are shown in Fig. 1 for all four sandstones. In this figure, the applied extensions according to Webb (2000) are also presented. The associated matching point saturations and capillary pressures are listed in Table 4. The measured $k_r - S$ data for both phases and the associated model relations for the four sandstones are shown in Fig. 2. As intended in the literature, it was assumed that the gas relative permeability reaches a value of 1 at the irreducible aqueous phase saturation in the VG-M, BC-B, VG-C, and VG-hMC models. The fitted gas relative permeability relations for the VG-EPL and BC-vC models assume a linear segment between the endpoint relative permeability at the irreducible water saturation and a relative permeability of 1 at $S_l = 0$, similar to what was used by Mathias et al. (2013) and Krevor et al. (2012).

Test Case Description

The Test Case defined by Mathias et al. (2013) was used to simulate 1-D and 2-D CO_2 injection in homogeneous reservoirs. The 2-D simulations were included to investigate the effects of buoyancy on the plume development. Test Case details are shown in Table 5. In the horizontal direction of both the 1-D and 2-D cases, a variable grid size was employed ranging from a minimum length of 0.5 cm adjacent to injection boundary to a maximum length of 10 m. The small grid cells near the injection boundary were needed to obtain monotonically increasing pressures, as observed by Pickup et al. (2012) and Mathias et al. (2013). For the 2-D simulations, a uniform grid size of 1 m was used in the vertical direction,

which is equal to the fine grid size used by Yamamoto and Doughty (2011) in their investigation of gridding effects. The injection was assumed to be uniform over the vertical length or the reservoir.

3. Results and Discussion

Capillary Pressure and Relative Permeability Relations

The BC curves (red lines) in Fig. 1 are the fitted expressions (Krevor et al., 2012) to the experimental $S - P_c$ data. These curves are used in the BC-B and BC-vC models. The curves indicate that the Berea and Paaratte rocks have similar characteristics and that the Mt. Simon sandstone has the largest P_e value. The VG curves used in the VG-M, VG-C, and VG-hMC models (black lines) are very close to the BC curves, except at high aqueous phase saturations. Under these conditions, the differences are the result of the entry pressure value, which is zero for the VG relations but greater than zero for the BC relation. The VG curve used in the VG-EPL model (blue lines) is different than for the other models because the endpoint aqueous phase saturation (S_{l0}) of the $k_r - S$ relation is used as the irreducible saturation (S_{li}). For this model, aqueous phase displacement is harder than for the other VG models as for a given capillary pressure, the aqueous saturations are larger. The effects of the Webb extension are the largest (blue dashed lines) for the VG-EPL model because of the large saturation matching points (Table 4).

In general, the fitted VG-EPL and BC-vC relative permeability relations have, as expected, good matches with the experimental data, making the BC-vC model the only model with good fits to both the $S - P_c$ and $k_r - S$ experimental data. For that reason, the simulation results for this model will be used as a reference in the discussions.

The $k_{rg} - S$ curves for the models not fitted to experimental data (VG-M, BC-B, VG-C, and VG-hMC) are relatively close for each of the sandstones, with a few notable exceptions. The Mualem $k_{rg} - S$ relation, as used in the VG-M model, overestimates the experimental data for all sandstones. The shape of the curve is convex for all rock types, which is inconsistent with the concave shapes that are typically obtained in the laboratory (e.g., Bennion and Bachu, 2010; Benson et al., 2013; Muller, 2011). The convex shape of the Mualem $k_{rg} - S$ curves is related to the relatively low n_v values, ranging from 1.669 for the Mt. Simon to 2.266 for the Paaratte sandstone (Table 3). Using the VG-M $k_{rg} - S$ equation (Table 1), it can be shown that a concave shape similar to the other $k_{rg} - S$ relations would only be reached for relatively large n_v values (i.e., $n_v > 8$), which are indicative of highly uniform porous media and are much larger than typical n_v values for sandstones (Schroth et al., 1996). This discrepancy suggests that the use of the Mualem $k_{rg} - S$ relation in the VG-M model may not be appropriate to describe $scCO_2$ relative permeability for the considered rocks.

Although the differences are less than for the VG-M model, the VG-EPL $k_{rg} - S$ curve deviates from the other models for the Tuscaloosa and Mt. Simon sandstone. The main reason for the differences is that the EPL fit does not include the range below the endpoint saturation, for which a linear relation was assumed. For the Tuscaloosa sandstone, which has a very low endpoint saturation (Fig. 2c), the k_{rg} values are larger than for the other models in that range. The EPL fit for the Mt. Simon (Fig. 2d) deviates from the other models because of the combination of the moderate endpoint saturation for the EPL fit and the relatively high irreducible water saturation used for the other models. As a result the k_{rg} values are larger than for the other models above the endpoint

saturation and smaller below.

For the $k_{rl} - S$ relations, there is more variation between the models that do not use direct fits to the data (VG-M, BC-B, VG-C, and VG-hMC). The Corey model consistently overestimates the values for all models. Given that the differences with the Corey model and the models directly fitted to the experimental data (VG-EPL and BC-vC) are substantial for all considered sandstones and biased towards larger k_{rl} values, the Corey $k_{rl} - S$ relation may not be a good choice for $scCO_2$-brine displacement simulations. For the non-fitted models, the Burdine $k_{rl} - S$ curves used in the BC-B also overestimate k_{rl} values for most of the sandstones. The Mualem $k_{rl} - S$ curves, used in the VG-M and VG-hMC model, appear to provide the best matches with experimental data, with the exception of the Berea sandstone. Combining this observation with the previous finding that the Corey $k_{rg} - S$ relation provide good matches with the experimental data, the use of the VG-hMC model appears to be a reasonable approach for the models without fitted relative permeability relationships.

For the Berea sandstone (Fig. 2a), it is noted that the $k_{rl} - S$ BC-B and BC-vC relations overlap due the use of $\lambda = 0.67$ in the Burdine and $N_{l-vC} = 6.0$ in the variable Corey relations, respectively (Table 3), yielding almost identical expressions.

1-D Simulations

Spatial distributions of gas saturations, relative permeabilities, and pressures at the end of the injection period are shown in Figs. 3, 4, 5, and 6 for the Berea, Paaratte, Tuscaloosa, and Mt. Simon reservoirs, respectively. To a large degree, the results can be explained using the $k_r - S - P_c$ relations shown in Figs. 1 and 2. Using the VG-M model, the injected $scCO_2$ migrates considerably further into all

reservoirs compared to all other models (Figs. 3a, 4a, 5a, and 6a). In addition, the k_{rg} values for the VG-M model at all locations are always larger (Figs. 3b, 4b, 5b, and 6b) and the gas pressures smaller (Figs. 3c, 4c, 5c, and 6c) than for the other models. These results can be primarily attributed to the much larger k_{rg} values, as a function of S_g, for the VG-M model compared to the others (Fig. 2).

For each of the sandstones, the horizontal plume extent was the least for the approach using the VG-C model (Figs. 3a, 4a, 5a, and 6a). Consequently, the average $scCO_2$ saturation over the plume length was the largest for this modeling approach. The main reason for this behavior is the use of the Corey $k_{rl} - S$ relation (Table 3), yielding considerable larger k_{rl} values of the pertinent saturation range than the other models. The aqueous phase is therefore easier to be displaced for this model, resulting in larger average gas saturations and a smaller plume extent. The relative results for each sandstone using the VG-C model, compared to the other models, is related to the fact that the Corey $k_{rl} - S$ relation is the same for each rock (Table 1) and produces values that are consistently larger than for the other models. Given that the differences with the Corey model and the models directly fitted to the experimental data (VG-EPL and BC-vC) are substantial and biased towards larger k_{rl} values, the Corey $k_{rl} - S$ relation does not appear to be a good choice for $scCO_2$-brine displacement simulations.

The gas saturation figures (Figs. 3a, 4a, 5a, and 6a) indicate that for all $k_r - S - P_c$ models simulations a dry-out zone develops, with a relatively rapid decrease in saturation with distance from the injection location. The shape of the curves is similar to simulation results obtained by Mathias et al. (2013) for the same test case. The dry-out zone for each simulation and rock type is fairly consistent and ranges from approximately 75 to 100 m after 30 years of injection.

Away from the dry-out zone, the $scCO_2$ saturations are relatively low, with the lowest saturations always obtained with the VG-M model and the highest with the VG-C model. For each model, these low saturations in this zone mostly correlate with capillary pressures smaller than the Webb (2000) matching point capillary pressures, even for the VG-EPL with considerably larger S_{li} values. These observations indicate that the extended part of the $S - P_c$ relations, below the matching point saturation, (Fig. 1) was not used for most of each plume except the dry-out zone.

The results for the Berea sandstone show relatively small differences in plume extent, saturations, and pressures (Fig. 3) for the BC-B, VG-hMC, VG-EPL, and BC-vC models. The results for the BC-B and BC-vC models are nearly the same because the k_{rl} values are the same and the k_{rg} values are very close (Fig. 2a) for this particular rock. The formation pressures during injection are only up to ~0.5 MPa larger than the initial pressure of 10 MPa (Fig. 3c) with differences smaller than ~0.2 MPa between the models. This result is consistent with the high permeability of this sandstone (914 mD) and indicates that the imposed injection rate of 15 kg/s can be easily handled by a reservoir with similar characteristics. Of interest is that the relative position of the pressure plots for the six models (Fig. 3c) is the inverse of the relative positions of the k_{rg} relations (Fig. 3b). This observation is also valid for all other considered sandstone, although the relative position is different for each of them. For the Berea sandstone, the highest pressures are obtained for the VG-hMC model, which has both the lowest k_{rl} and k_{rg} values for the saturation range applicable to most of the plume (Fig. 2a).

Compared to the Berea simulations (Fig. 3a), the results for the Paaratte reservoir generally show smaller plumes (Fig. 4a), primarily because of its larger porosity (0.283 for Paaratte vs. 0.221 for Berea). The larger porosity yields more

compact saturation distributions at pressures that are even lower than for the Berea simulations (Fig. 4c). In contrast to what was observed for the Berea simulations, the BC-B and BC-vC models for the Paaratte sandstone do not produce identical results. For this rock type, the fitted k_{rl} and k_{rg} values for the BC-vC model are considerably smaller than for the non-fitted BC-B model (Fig. 2b), leading to a smaller plume extent and larger formation pressures. The two models with relative permeability relations fitted to experimental data, BC-vC and VG-EPL, yielded similar results at slightly higher pressures (Fig. 4c) and at lower k_{rg} values (Fig. 4b) than the other models. The simulated larger resistance to injection for these two models is consistent with the lower relative permeability values for both phases over the predominant saturation range of the $scCO_2$ plume (Fig. 2b).

The results for the Tuscaloosa reservoir, having a moderate permeability of 220 mD, show more variability (Fig. 5) than for the highly permeable Berea and Paaratte cases. For this sandstone, especially the VG-EPL results are different than those for the more permeable reservoirs. Fig. 5a shows relative low and almost constant gas saturations beyond the dry-out zone with k_{rg} values less than 0.05. In addition, the gas pressures in the formation are considerably larger than those for the other models. The reason for the different VG-EPL results is associated with the low endpoint saturation and relative permeability of the k_{rg} relations and the extremely low fitted k_{rg} values, even at S_l values above 0.8 (Fig. 2c). Under these conditions, the aqueous phase is difficult to displace by $scCO_2$, resulting in relatively large pressures to force the nonwetting fluid into the formation. This observed behavior illustrates the need to obtain reliable relative permeability relations for a potential reservoir, beyond permeability and porosity data. Based only on the measured permeability and porosity

information, and using a relative permeability model not fitted to measurement data, predicted gas pressures after 30 years of injection are only ~2 MPa larger than the formation pressure, which are typically acceptable for reservoir injection. However, when using the VG-EPL model, the relative permeability limitations of this sandstone become apparent, leading to much larger formation gas pressures. Interestingly, the other model that uses fitted relative permeability relations, BC-vC, does not produce similarly high pressures or low saturations as the VG-EPL model. The differences between these models result from the $S - P_c$ relations shown in Fig. 1c. The very large endpoint saturation ($S_{i0} = 0.7030$) yields a retention relation where the aqueous phase is much harder to replace by $scCO_2$ than for the BC $S - P_c$ relation. For the Berea (Fig. 1a) and Paaratte (Fig. 1b) formations, this effect was much less pronounced because the $S - P_c$ relations are much closer together over the predominant saturation range of the plume beyond the dry-out zone. Given the large differences in results between the BC-vC and VG-EPL models for this sandstone, with a low relative permeability endpoint at a high aqueous phase saturation, additional research is needed to determine if using VG-EPL $S - P_c$ relations according to Mathias et al. (2013) is appropriate.

The gas saturations for the Mt. Simon simulations (Fig. 6a) are similar to the Berea and Paaratte results and do not show the larger variability observed for the Tuscaloosa formation. A major difference with the other simulations is that the low permeability of the Mt. Simon (7.5 mD) leads to very large gas pressures, as is shown in Fig. 6c. Although the simulated pressures are obviously too large for actual injection at the imposed rate (15 kg/s), the simulation results are still of interest in this analysis. The gas saturation plots indicate plume extents and saturations comparable to the Paaratte simulations for all models, although the

Paaratte has a larger porosity. The reason that similar plume extents are obtained for these different conditions is related to the high gas pressures needed to inject the $scCO_2$ at the prescribed rate in the Mt. Simon. For these higher pressures, the aqueous phase solubility is considerably larger, yielding less CO_2 to migrate in the supercritical phase.

The saturation plots in Figs. 3a, 4a, 5a, and 6a show that the VG-hMC results are reasonably close the BC-vC model, consistent with the observation that the non-fitted $k_{rg} - S$ and $k_{rl} - S$ relations in the VG-hMC model have mostly good matches with the experimental data (Fig. 2). Therefore, the use of the VG-hMC model appears to be the most reasonable of the four models that do not have fitted relative permeability relationships.

2-D Simulations

In this section, the results of the 2-D radial simulations are presented. First, horizontal plume extents are shown as a function of time. Then, gas saturations of selected simulations at the end the 30-year injection period are discussed. Next, formation pressures distributions are presented, followed by a discussion of the dry-out zone formation.

The relative positions of the horizontal plume extents (Fig. 7) are similar as for the 1-D simulations. The plots in Fig. 7 show that the predicted horizontal plume extents of the various models are relatively close, except for the VG-M model. With the exception for the Tuscaloosa sandstone, where the VG-EPL model produced the smallest plume, the application of the VG-M model resulted in the largest and the VG-C model in the smallest plumes. The reasons for the VG-M and VG-C model behavior have been discussed in the previous section.

The explanation for the Tuscaloosa exception is given in the description of Fig. 10 below.

In Figs. 8 through 11, final gas saturation distributions obtained with the BC-vC, VG-M, and VG-EPL models are shown. The BC-vC model uses fitted capillary pressure and relative permeability relations, the VG-M model always produced the largest plumes, and the VG-EPL results typically deviate from the other models. The saturation distributions resulting from the remaining models (i.e., BC-B, VG-hMC, and VG-C) are similar to the VG-M simulations, although the plume extents are smaller. The shape of $scCO_2$ plumes in Figs. 8, 9, and 10 indicate strong buoyancy effects for the injections in the more permeable Berea, Paaratte, and Tuscaloosa sandstones. On the other hand, the vertical migration component was considerably smaller for the injection in the low-permeability Mt. Simon (Fig. 11). In general, due to the buoyancy effects associated with less dense $scCO_2$ in the reservoirs, the simulated 2-D plume extents (Fig. 7) are larger than for the 1-D simulations (Figs. 3-6), with the exception of the plumes for the Mt. Simon simulations. The differences between 1-D and 2-D plume extents are the largest for the VG-M model, showing 2-D plume extents that are ~1300 and ~1000 m larger than the 1-D plume lengths for Berea and Paaratte sandstone, respectively. For the much tighter Mt. Simon sandstone, the differences are much smaller (only ~200 m for the VG-M model) as its lower permeability leads to reduced vertical transport. For the other Mt. Simon model simulation similar observations can be made except that the differences between the 2-D and 1-D results are less.

As can be seen in Figs. 8 – 10, the appearance of the plumes generated with VG-EPL models is much different for all sandstones, except for the Mt. Simon where the plume looks similar to the BC-vC plume. For the Berea and Paaratte VG-EPL simulation, a large portion of the plume has relatively uniform gas

saturations, with values less than 0.55 outside the dry-out zones (Figs. 8c and Fig. 9c), compared to more gradually changing saturations for the other model simulations (Figs. 8a and 8b for Berea; Figs 9a and 9b for Paaratte). The reason for the more uniform appearance is related to the $S - P_c$ relations used for the VG-EPL simulations (Figs. 1a and 1b). The pressures needed to inject the imposed 15 kg/s $scCO_2$ into these high-permeability sandstones are low (see an example in Fig. 12 for the Berea BC-vC simulation), and therefore the capillary pressures outside of the dry-out zone are relatively small, resulting in gas saturations mostly below 0.5 for both sandstones. For the other models, the range in gas saturations at lower capillary pressures is larger, resulting in values up to 0.8 outside the dry-out zones. The pressure distributions for the high-permeable Berea and Paaratte formations are similar for all models with only small deviations from hydrostatic conditions near the injection location (Fig. 12).

The VG-EPL model for the Tuscaloosa sandstone produces a relatively uniform plume with gas saturations mostly between 0.2 and 0.25 outside the dry-out zone (Fig. 10c). The figure also shows that although the Tuscaloosa sandstone is considered to be moderately permeable (Krevor et al., 2012), strong capillarity results in multiphase flow effects that minimize buoyancy in the vertical direction. The totally different appearance of the VG-EPL plume (Fig. 10c), compared to the other plumes (Figs. 10a,b), is the result of the combined effects of the rapidly decreasing k_{rl} during drainage at high aqueous phase saturations (Fig. 2c), and $S - P_c$ relation (Fig. 1c) that is strongly affected by the imposed large irreducible water saturation. The k_{rl} at high aqueous phase saturations is overestimated by all models except for the BC-vC and VG-EPL models. The models that do not using fitted k_r expressions predict formation pressures (e.g., Fig. 13b) that are larger than for the Berea and Paaratte injections (Fig. 12) with

values almost inversely proportional to the formation permeability. The pressure distribution of the Tuscaloosa VG-EPL simulations shows near-vertical isobars (Fig. 13c) in the first 1500 m at the end of the injection period, with maximum pressures near 13.5 MPa. The larger pressures are needed to overcome the mentioned relative permeability and capillary pressure restrictions. The BC-vC pressures (Fig. 13a) are only slightly larger than the VG-M results shown in Fig. 13b. For this model, the $S - P_c$ relation uses a much smaller S_{li} (0.05) than what is used for the VG-EPL model (0.703), resulting in the need of much smaller gas pressures for brine displacement.

The gas saturation plots for the Mt. Simon (Fig. 11) are of interest because they depict distributions for hypothetical cases where the injection rate can only be achieved through very large injection pressures, ranging from approximately 40 to 55 MPa, depending on the used model (Fig. 14). The low sandstone permeability reduces the potential for vertical flow due to buoyancy and the resulting isobars are nearly vertical for several kilometers from the injection location. Opposed to what was found for the other sandstones, the simulated Mt. Simon gas saturations for the VG-EPL model (Fig. 11c) are close to the BC-vC results (Fig. 11a) because the differences in the $S - P_c$ relations used for these two models are the smallest (Fig. 2c).

Dry-out for the more permeable sandstone is comparable among the models, with saturation distributions strongly affected by buoyancy. Examples for Berea formation simulations are shown in Fig. 15. The only exception is observed for the VG-EPL model, where the fully desiccated zone extent only varies by about 20 m in the vertical direction after 30 years of injection (Fig. 15c). The occurrence of the sharp interface between the dry-out zone and the rest of the $scCO_2$ plume for the VG-EPL model is related to the $S - P_c$ curve (Fig. 1a), which has been

explained in the discussion of gas distributions in Fig. 8. To relate dry-out for the different sandstones using the same model, the VG-M simulation results shown in Fig. 16 should be compared to Fig. 15a. The four figures (Fig. 15a, 16a, 16b, and 16c) show the clear effect of permeability on the shape of the dry-out zone. A reduction of the formation permeability reduces the vertical saturation differences, with the dry-out zone for the low-permeability Mt. Simon to be nearly vertical.

4. Summary and Conclusions

The injection behavior of $scCO_2$ into homogeneous reservoirs was compared for six $k_r - S - P_c$ models using hydraulic property data from four well-characterized sandstones. All models used $S - P_c$ relations fitted to laboratory capillary pressure data, with the exception for the irreducible aqueous phase saturation in the VG-EPL model, which was the same as the endpoint saturation for the associated $k_{rg} - S$ relation. These values for the VG-EPL model were therefore much larger than for the other models. Of the six $k_r - S - P_c$ models, only the VG-EPL and BC-vC models use fitted $k_r - S$ relations to laboratory relative permeability data, making the BC-vC model the only one with fits to both the capillary pressure and relative permeability data. The $k_r - S$ and $S - P_c$ relations of the VG-M and BC-B models are coupled through a pore-geometry parameter obtained for the $S - P_c$ fit with the experimental data. The VG-C model uses fully empirical $k_r - S$ relations, while the VG-hMC model uses a hybrid $k_r - S$ formulation with and coupled Mualem-type $k_{rl} - S$ relation and an empirical Corey type $k_{rg} - S$ relation.

The simulation results show that, depending on the $k_r - S - P_c$ model, large

variations in plume extent and saturation distribution are predicted. The fully fitted BC-vC model yielded intermediate results for all sandstones. In all cases, the VG-M model predicts plumes that are considerably larger than for the other models due to the overestimation of the k_{rg}. For the 2-D simulations, the differences are more enhanced due to buoyancy effects and are related to the shape of the Mualem $k_{rg} - S$ relation, which is different from those of the other models and the experimental data. The discrepancy is an indication that the Mualem $k_{rg} - S$ relations may not be appropriate for $scCO_2$ injection simulations. The horizontal plume extent was the smallest for most of the VG-C simulations. The main reason for this result is that the empirical Corey $k_{rl} - S$ relation yields much larger k_{rl} values than the other models and the experimental data. As a consequence, the aqueous phase is easier to displace using this model, resulting in larger average $scCO_2$ saturations and an associated smaller plume. These results illustrate the point that the use of relative permeability models based on capillary pressure data only or on empiricism may result in considerable uncertainty.

Although in general it is to be preferred to use a model fitted to quality experimental data, such as the BC-vC model, the VG-hMC model, which only uses fitted $S - P_c$ relations, produced results that relatively close to the BC-vC results for most sandstones. Of the four models that do not use fitted $k_r - S$ relations (VG-M, BC-B, VG-C, and VG-hMC), the use of the popular VG-hMC model appears to be the most reasonable, because good matches of both the Mualem $k_{rl} - S$ and the Corey $k_{rg} - S$ relations to the experimental data are obtained.

The 2-D plumes generated with the VG-EPL model were always different in shape and saturation distribution than the plumes obtained with the other

models. For the more permeable sandstone (Berea and Paaratte), the VG-EPL plumes outside the dry-out zone have uniform gas saturations. The uniformity is related to the relatively small capillary pressures needed to inject the $scCO_2$ into these reservoirs. Due to the use of relatively high irreducible aqueous phase saturations, the ranges in the gas saturations are therefore smaller. The VG-EPL plume generated for the Tuscaloosa reservoir is characterized by a very low, uniform saturation as a result of the rapidly declining k_{rl} with increasing $scCO_2$ saturation and the very high irreducible aqueous phase. Because of these characteristics, $scCO_2$ injection requires considerable larger pressures than for the other models because it is much more difficult to displace the aqueous phase. The different results obtained with the VG-EPL model for these sandstones suggest that this model should be used with caution. A different way to assign the irreducible aqueous phase saturation value to the $S - P_c$ relations may be required, maintaining consistency with the endpoint saturation used in the endpoint power law $k_{rg} - S$ relation.

The simulations for the Tuscaloosa reservoir demonstrate the need to obtain relative permeability data beyond permeability and porosity. For this particular non-uniform sandstone, the permeability and porosity indicate that there should not be injectivity issues. However, the measured low endpoint k_{rg} and the rapidly declining k_{rl} lead to increased demands on the injection pressure that are not apparent when models are used that do not used fitted relative permeability data.

Given the respective over- and under-estimation of the plume extents with the VG-M and VG-C models for these nonhysteretic simulations, the results indicate that development of full hysteretic capabilities (entrapment and pore-geometry hysteresis) should not be based on these models. Current hysteretic

capabilities for $scCO_2$ injection and redistribution appear to have been developed for the VG-M model only (Doughty, 2007; 2010). A hysteretic implementation should ideally be based on a model like the BC-vC, which uses fits to both the capillary pressure and relative permeability data. Alternatively, a hysteretic VG-M model could be relatively easily modified into a VG-hMC model, which produced comparable results with the BC-vC model for most sandstones, by using hysteretic Corey instead of Mualem $k_{rg} - S$ relations.

The presented analysis and conclusions are only valid for the four sandstones characterized by Krevor et al. (2013). It is recommended that a similar approach would be conducted for other type rocks when comprehensive $k_r - S - P_c$ data become available.

Acknowledgments

Funding for this research was provided by the FutureGen 2.0 program, implemented under Cooperative Agreement DE-FE0001882 between the U.S. Department of Energy and the FutureGen Industrial Alliance, a non-profit membership organization created to benefit the public interest and the interests of science through research, development, and demonstration of near-zero emissions coal technology. For more information on FutureGen 2.0, please visit www.futuregenalliance.org. Pacific Northwest National Laboratory is operated by the Battelle Memorial Institute for the Department of Energy (DOE) under Contract DE-AC06-76RLO 1830.

References

Alkan, H., Cinar, Y., Ulker, E. 2010. Impact of capillary pressure, salinity and in situ conditions on CO2 injection into saline aquifers. Transport in Porour Media 84: 799-819.

Akbarabadi, M., Piri, M. 2013. Relative permeability hysteresis and capillary trapping characteristics of supercritical CO_2/brine systems: An experimental study at reservoir conditions. Adv. Water Resour. 52: 190-206.

Bachu, S. and Bennion, B. 2008. Effects of in-situ conditions on relative permeability characteristics of CO_2-brine systems. Environmental Geology 54, 1707-1722.

Bandilla, K.W., Celia, M.A., Elliot, T.R., Person, M., Ellet, K.M., Rupp, J.A., Gable, C., and Zhang, Y. 2012. Modeling carbon sequestration in the Illinois Basin using a vertically-integrated approach Computing and Visualization in Science 15 (1), 39-51.

Benisch, K., Bauer, S. 2013. Short- and long-term regional pressure build-up during CO_2 injection and its applicability for site monitoring. Int. J. of Greenhouse Gas Control 19, 220-233.

Bennion, B., Bachu, S. 2008. Drainage and imbibition relative permeability relations for supercritical CO_2/brine and H_2S/brine systems in intergranular sandstone, carbonate, shale, and anhydrite rocks. SPE Reservoir Evaluation & Engineering 11, 487-496.

Bennion, D.B., S. Bachu. 2010. Drainage and imbibition CO_2/brine relative permeability curves at reservoir conditions for high-permeability carbonate rocks. Paper presented at the SPE Annual Technical Conference and Exhibition. Florence, Italy, 19-22 September 2010.

Benson, S.M., Pini, R., Reynolds, C., Krevor, S. 2013. GCCSI Reports 2: Relative permeability analyses to describe multi-phase flow in CO_2 storage reservoirs. Global Carbon Capture and Storage Institute.

Benson, S.M., Hingerl, F., Zuo, L., Pini, R., Krevor, S., Reynolds, C., Niu, B., Calvo, R., Niemi, A. 2015. Relative permeability for multi-phase flow in CO_2

storage reservoirs. Part 2: Resolving fundamental issues and filling data gaps. Global Carbon Capture and Sequestration Institute.

Birkholzer, J.T., Zhou, Q., Tsang, C.F. 2009. Large-scale impact of CO2 storage in deep saline aquifers: a sensitivity study on pressure response in stratified systems. Int. J. Greenhouse Gas Control 3: 181-194.

Brooks, R.H., Corey, A.T. 1964. Hydraulic properties of porous media. Hydrology Papers 3 Fort Collins, Colorado: Colorado State University.

Burdine, N. T. 1953. Relative permeability calculations from pore size distribution data. Transactions of the American Institute of Mining and Metallurgical Engineers 198, 71-78.

Cameron, D.A., and Durlofsky, L.J. 2012. Optimization of well placement, CO_2 injection rates, and brine cycling for geological carbon sequestration. Int. J. of Greenhouse Gas Control 10, 100-112.

Chadwick, R.A., Williams, G.A., Williams, J.D.O., Noy, D.J. 2012. Measuring pressure performance of a large saline aquifer during industrial-scale CO_2 injection: The Utsira Sand, Norwegian North Sea. Int. J. of Greenhouse Gas Control 10: 374-388.

Class, H., Ebigbo, A., Helmig, R., Dahle, H.K., Nordbotten, J.M., Celia, M.A., Audigane, P., Darcis, M., Ennis-King, J., Fan, Y., Flemisch, B., Gasda, S.E., Jin, M., Krug, S., Labregere, D., Beni, A.N., Pawar, R.J., Sbai, A., Thomas, S.G., Trenty, L., and Wei, L. 2009. A benchmark study on problems related to CO2 storage in geologic formation. Comput. Geosc. 13: 409-434.

Corey, A.T. 1954. The interrelation between gas and oil permeabilities. Producer's Monthly 19(1), 38-42.

Court, B., Bandilla, K.W., Celia, M.A., Janzen. A., Dobossy, M., Nordbotten, J.M. 2012. Applicability of vertical-equilibrium and sharp-interface assumptions in CO_2 sequestration modeling. Int. J. Greenhouse Gas Control 10: 134-147.

DeHoff, K.J., Oostrom, M., Zhang, C., and Grate, J.W. 2012. Evaluation of two-phase relative permeability and capillary pressure relations for unstable displacements in a pore network. Vadose Zone J.,doi:10.2136/vzj2012.0024.

Doughty, C. 2007. Modeling geologic storage of carbon dioxide: Comparison of non-hysteretic and hysteretic characteristic curves. Energy Convers. and Management 48 (6), 1768-1781.

Doughty, C., Freifeld, B.M., and Trautz, R.C. 2008. Site characterization for CO_2 geologic storage and vice versa: the Frio brine pilot, USA as a test case. Environ. Geol. 54, 1635-1656.

Doughty, C. 2010. Investigation of CO_2 plume behavior for a large-scale pilot test of geologic carbon storage in a saline formation. Transport in Porous Media 82 (1), 49-76.

Dury, O., Fischer, U., Schulin, R. 1999. A comparison of relative nonwetting-phase permeability models. Water Res. Research 35: 1481-1493.

Ebigbo, A., Class, H., Helmig, R. 2007. CO_2 leakage through and abandoned well: problem oriented benchmarks. Comp. Geosciences 11: 103-115.

Espinet, A., Shoemaker, C., Doughty, C. 2013. Estimation of plume distribution for carbon sequestration using parameter estimation with limited monitoring data. Water Resources Research 49, 4442-4464.

Giorgis, T., Carpita, M., Battistelli, A. 2007. 2D modeling of salt precipitation during the injection of dry CO_2 in a depleted gas reservoir. Energy Convers.and Management 48 (6), 1816-1826.

Gor, G.Y., Elliot, T.R., Prevost, J.H. 2013. Effects of thermal stress on caprock integrity during CO_2 storage. Int. J. of Greenhouse Gas Control 12, 300-309.

Juanes, R., Spiteri, E.J., Orr Jr., F.M., Blunt, M.J. 2006. Impact of relative permeability hysteresis on geological CO_2 storage, Water Resour. Res., 42, W12418, doi:10.1029/2005WR004806.

Kim, K-Y., Han, W.S., Oh, J., Kim, T., Kim J-C. 2012. Characteristics of salt-precipitation and the associated pressure build-up during CO2 storage in saline aquifers. Transport in Porous Media 92, 397-418.

Kolditz, O., Bauer, S., Beyer, C., Bottcher, N., Dietrich, P., Gorke, U., Kalbacher, T., Park, C., Sauer, U., Schutze, C., Shao, H., Singh, A., Taron, J., Wang, W.,

Watanabe, N. 2012. A systematic approach for geologic CO_2 injection and storage. Environ. Earth. Sci. 67: 613-632.

Krevor, S.C. M., Pini, R., Zuo. L., Benson, S.M. 2012. Relative permeability and trapping of CO_2 and water in sandstone rocks at reservoir conditions. Water Resour. Res. 48.

Lenhard, R. J., Parker, J.C. 1987. A model for hysteretic constitutive relations governing multiphase flow. 2. Permeability-Saturation relations. Water Resour. Research 23 (12), 2197-2206.

Lenhard, R.J., Parker, J.C, and Mishra, S. 1989. On the correspondence between Brooks-Corey and van Genuchten models. J. of Irrigation and Drainage Engineering 115: 744-751.

Liu, F., Peng, L., Zhu, C., Y. Xiao. 2011. Coupled reactive flow and transport modeling of CO2 sequestration in the Mt. Simon sandstone formation, Midwest, U.S.A. Int. J. of Greenhouse Gas Control 5, 294-307.

Lu, C., Lee, S-Y, Han, W.S., McPherson, B.J., Lichtner, P.C. 2009. Comments on "Abrupt-interface solution for carbon dioxide injection into porous media" by M. Dentz and D. Tartakovsky. Transp. Porous Media 79: 29-37.

Mathias, S.A., Gluyas, J.G., Gonzalez Martinez de Miguel, G.J., Bryant, S.L., Wilson, D. 2013. On relative permeability uncertainty and CO_2 injectivity estimation for brine aquifers. Int. J. of Greenhouse Gas Control 12, 200-212.

Middleton, R.S., Keating, G.N., Stauffer, P.H., Jordan, A.B., Viswanathan, H.S., Kang, Q.J., Carey, J.W., Mulkey, M.L., Sullivan, E.J., Chu, S.P., Esposito, R., Meckel, T.A. 2012. The cross-scale science of CO2 capture and storage: from pore scale to regional scale. Energy Environmental Science 5, 7328-7345.

Mitiku, A.B., Bauer, S. 2013. Optimal use of a dome-shaped anticline structure for CO_2 storage: a case study in the North German sedimentary basin. Environ. Earth Sciences 70 (8), 3661-3673.

Mualem, Y. 1976. New model for predicting hydraulic conductivity of unsaturated porous-media. Water Resour. Research 12 (3), 513-522.

Muller, N. 2011. Supercritical CO_2-brine relative permeability experiments in reservoir rocks – Literature review and recommendations. Transport in Porous Media 87: 367-383.

Nitao, J.J. 1988. Numerical modeling of the thermal and hydrological environment around a nuclear waste package using the equivalent continuum approximation: horizontal emplacement. UCID-2144. Lawrence Livermore National Laboratory, Livermore, CA.

Oldenburg, C.M., Pruess, K., and Benson, S.M. 2001. Process modeling of CO2 injection into natural gas reservoirs for carbon sequestration and enhanced gas recovery. Energy Fuels 15: 293–298.

Okwen, R., Stewart, M., Cunningham, J. 2011. Effect of well orientation (vertical vs. horizontal) and well length on the injection of CO_2 in deep saline aquifers. Transport in Porous Media 90 (1), 219-232.

Orr Jr., F.M. 2007. Theory of Gas Injection Processes. Copenhagen, Denmark: Tie-Line Publications.

Parker, J.C. and Lenhard, R.J. 1987. A model for hysteretic constitutive relations governing multiphase flow. 1. Saturation-pressure relations. Water Resour. Res. 23:2187-2196.

Perrin, J-C, Benson, S. 2010. An experimental study on the Influence of sub-core scale heterogeneities on CO_2 distribution in reservoir rocks. Transport in Porous Media 82 (1), 93-109.

Pham, V. T. H., Riis, F., Gjeldvik, I. T., Halland, E. K., Tappel, I. M., Aagaard, P. 2013. Assessment of CO_2 injection into the south Utsira-Skade aquifer, the North Sea, Norway. Energy 55, 529-540.

Pickup, G., Jin, M., Mackay, E.J. 2011. A sensitivity study on CO2 storage in saline aquifers. In: SPE EUROPEC/EAGE Annual Conference and Exhibition, Vienna, Austria. Soc. Petrol. Eng. Paper 143054.

Pini, R., Krevor, S.C.M., Benson, S.M. 2012. Capillary pressure and heterogeneity for the CO2/water system in sandstone rocks at reservoir conditions. Advances in Water Resources 38, 48-59.

Pruess, K., J. Garcia. 2002. Multiphase flow dynamics during CO_2 disposal into saline aquifers. Environ. Geology 42 (2-3), 282-295.

Pruess, K., Muller, N. 2009. Formation dry-out from CO_2 injection into saline aquifers: 1. Effects of solids precipitation and their mitigation. Water Resour. Research 45.

Pruess, K., Oldenburg, C.M., Moridis, G., 1999. TOUGH2 User's Guide, Version 2.0. Report LBNL-43134, Lawrence Berkeley National Laboratory, Berkeley, CA, USA.

Pruess, K., Spycher, N., 2007. ECO2N – A fluid property module for the TOUGH2 code for studies of CO_2 storage in saline aquifers. Energy Conv. and Management 48, 1761–1767.

Pruess, K., Xu, T., Apps, J., Carcia, J. 2003. Numerical modeling of aquifer disposal of CO_2. Soc. Petrol. Eng. J. 8, 49-60.

Rasmussen, K., Tsang, C-F., Tsang, Y., Rasmussen, M., Pan, L., Fagerlund, F., Bensabat, J. Niemi, A. 2014. Distribution of injected CO_2 in a stratified saline reservoir accounting for coupled wellbore-reservoir flow. Greenhouse Gases Science and Technology 4: 1-18.

Ruprecht, C., Pini, R., Falta, R., Benson, S., Murdoch, L. 2014. Hysteretic trapping and relative permeability if sandstone at reservoir conditions. Int. J. of Greenhouse Gas Control 27: 15-27.

Rutqvist, J., Birkholzer, J. T., Tsang, C.F. 2008. Coupled reservoir-geomechanical analysis of the potential for tensile and shear failure associated with CO_2 injection in multilayered reservoir-caprock systems. Int. J. of Rock Mechanics and Mining Sciences 45 (2), 132-143.

Sakurai, S., Ranakrishnan T.S., A. Boyd, N. Mueller, S.D. Hovorka. 2005. Monitoring saturation changes of CO2 sequestration: petrophysical support of the Frio brine pilot experiment. Paper presented at 46th Annual Logging Symposium, 26-29 June 2005, at New Orleans, LA.

Schnaar, G., Digiulio, D.C. 2009. Computational modeling of the geological sequestration of carbon dioxide. Vadose Zone J. 8: 389-403.

Schroth, M.H., Ahearn, S.J., Selker, J.S. and Istok, J.D. 1996. Characterization of Miller-similar silica sands for laboratory hydrologic studies. Soil Sci. Soc. Am. J. 60: 1331-1339.

Span, R., and W. Wagner. 1996. A new equation of state for carbon dioxide covering the fluid region from the triple-point temperature to 1100° K at pressure up to 800 MPa. J. Phys. Chem. Ref. Data 25(6): 1509-1596.

van Genuchten, M. T. 1980. A closed-form equation for predicting the hydraulic conductivity of unsaturated soils. Soil Sc. Society of America J. 44 (5), 892-898.

Vilarrasa, V. 2014. Impact of CO_2 injection through horizontal and vertical wells on the caprock mechanical stability. Int. J. of Rock Mechanics and Mining Sciences 66, 151-159.

Yamamoto, H., Zhang, K., Karasaki, K., Marui, A., Uehara, H., and Nishikawa, N. 2009. Numerical investigation concerning the impact of CO2 geologic storage on regional groundwater flow. Int. J. of Greenhouse Gas Control 3:586-599.

Yamamoto, H. and Doughty, C. 2011. Investigation of gridding effects for numerical simulations of CO2 geologic sequestration. Int. J. of Greenhouse Gas Control 5:975-985.

Webb, S.W. 2000. A simple extension of two-phase characteristic curves to include the dry region. Water Resour. Res. 36: 1425-1430.

White, M.D., Oostrom, M. 2006. STOMP Subsurface Transport Over Multiple Phases, Version 4.0, User's Guide. Pacific Northwest National Laboratory, Richland, WA.

White, M.D., Bacon, D.H., McGrail, B.P., Watson, D.J.., White, S.K., Zhang, Z.F. 2010. STOMP Subsurface Transport Over Multiple Phases, STOMP-CO2 nd STOMP-CO2e Guide.Version 1.0. PNNL-21268. Pacific Northwest National Laboratory, Richland, WA.

Xu, T.F., Apps, J.A., Pruess, K., Yamamoto, H. 2007. Numerical modeling of injection and mineral trapping of CO_2 with H_2S and SO_2 in a sandstone formation. Chemical Geology 242 (3-4), 319-346.

Xu, T., Kharaka, Y.K., Doughty, C., Freifeld, B.M., Daley, T.M. 2010. Reactive transport modeling to study changes in water chemistry induced by CO_2 injection at the Frio-I Brine Pilot. Chemical Geology 271 (3-4), 153-164.

Zhang, Z., Agarwal, R. 2013. Numerical simulation and optimization of CO_2 sequestration in saline aquifers. Computers & Fluids 80, 79-87.

Zhou, Q., Birkholzer, J.T., Mehnert, E., Lin, Y., Zhang. K. 2010. Modeling basin- and plume-scale processes of CO_2 storage for full-scale deployment. Ground Water 48 (4), 494-514.

1 **Table 1.** Overview of the $k_r - S - P_c$ models.

2

Model	$S - P_c$	$k_r - S$
VG-M (van Genuchten – Mualem)	$\bar{S}_l = \left[1 + \alpha P_c^{\ n_v}\right]^{-m_v}$ or $\bar{S}_l = \left[1 + \left(\frac{P_c}{P_o}\right)^{n_v}\right]^{-m_v}$	For $S_l > S_{li}$: $k_{rl} = \bar{S}_l^{\ 1/2}\left[1 - \left(1 - \bar{S}_l^{\ 1/m_v}\right)^{m_v}\right]^2$ $k_{rg} = \bar{S}_g^{\ 1/2}\left[\left(1 - \bar{S}_l^{\ 1/m_v}\right)^{m_v}\right]^2$ For $S_l \le S_{li}$: $k_{rl} = 0$; $k_{rg} = 1$
BC-B (Brooks-Corey – Burdine)	$\bar{S}_l = \left(\frac{P_c}{P_e}\right)^{-\lambda}$	For $S_l > S_{li}$: $k_{rl} = \bar{S}_l^{\ (3+2/\lambda)}$ $k_{rg} = \bar{S}_g^{\ 2}\left[1 - \bar{S}_l^{\ (1+2/\lambda)}\right]$ For $S_l \le S_{li}$: $k_{rl} = 0$; $k_{rg} = 1$
VG-C (van Genuchten – Corey)	$\bar{S}_l = \frac{S_l - S_{li}}{1 - S_{li}}$	For $S_l > S_{li}$: $k_{rl} = \bar{S}_l^{\ 4}$ $k_{rg} = \bar{S}_g^{\ 2}\left[1 - \bar{S}_l^{\ 2}\right]$ For $S_l \le S_{li}$: $k_{rl} = 0$; $k_{rg} = 1$
VG-hMC (van Genuchten – hybrid Mualem-Corey)	$\bar{S}_l = \left[1 + \alpha P_c^{\ n_v}\right]^{-m_v}$	For $S_l > S_{li}$: $k_{rl} = \bar{S}_l^{\ 1/2}\left[1 - \left(1 - \bar{S}_l^{\ 1/m_v}\right)^{m_v}\right]^2$ $k_{rg} = \bar{S}_g^{\ 2}\left[1 - \bar{S}_l^{\ 2}\right]$ For $S_l \le S_{li}$: $k_{rl} = 0$; $k_{rg} = 1$
VG-EPL (van Genuchten – Endpoint Power Law)	$\bar{S}_l = \left[1 + \alpha P_c^{\ n_v}\right]^{-m_v}$	For $S_l > S_{l0}$: $k_{rl} = k_{rl0-EPL}\left(\frac{S_l - S_{l0}}{1 - S_{l0}}\right)^{N_{l-EPL}}$ $k_{rg} = k_{rg0-EPL}\left(\frac{S_g}{1 - S_{l0}}\right)^{N_{g-EPL}}$ For $S_l \le S_{l0}$: $k_{rl} = 0$; $k_{rg} = 1 - \left(\frac{1 - k_{rg0-EPL}}{S_{l0}}\right)S_l$

BC-vC (Brooks-Corey – variable Corey)	$\bar{S}_l = \left(\frac{P_c}{P_e}\right)^{-\lambda}$	For $S_l > S_{li}$: $k_{rl} = \bar{S}_l^{N_{l-vC}}$ $k_{rg} = k_{rg0-vC}\bar{S}_g^{\,2}\left[1-\bar{S}_l^{N_{g-vC}}\right]$ For $S_l \le S_{li}$: $k_{rl} = 0$; $k_{rg} = 1-\left(\frac{1-k_{rg0-vC}}{S_{li}}\right)S_l$

1 $\bar{S}_l$, $\bar{S}_g$, and P_c are defined as, respectively:

2

3 $\bar{S}_l = \frac{S_l - S_{li}}{1-S_{li}}$, $\bar{S}_g = \frac{S_g}{1-S_{li}}$, and $P_c = P_g - P_l$

Table 2. Rock porosity and permeability (after Krevor et al., 2012)

Name	**Porosity (-)**	**Absolute Permeability (mD)**
Berea	0.221	914
Paarette	0.283	1156
Tuscaloosa	0.236	220
Mt. Simon	0.244	7.5

Table 3. Parameter values used for the $k_r - S - P_c$ models simulations.

	Berea		**Paaratte**	
Model	$S - P_c$	$k_r - S$	$S - P_c$	$k_r - S$
VG-M	$\alpha = 2.4 \times 10^{-4}$ 1/Pa $n_v = 1.864$ $m_v = 0.464$ $S_{li} = 0.11$	$m_v = 0.464$	$\alpha = 2.9 \times 10^{-4}$ 1/Pa $n_v = 2.266$ $m_v = 0.559$ $S_{li} = 0.05$	$m_v = 0.559$
BC-B	$P_e = 2.5 \times 10^3$ Pa $\lambda = 0.67$ $S_{li} = 0.11$	$\lambda = 0.67$	$P_e = 2.1 \times 10^3$ Pa $\lambda = 0.9$ $S_{li} = 0.05$	$\lambda = 0.9$
VG-C	as in VG-M		as in VG-M	
VG-hMC	as in VG-M	k_{rl}: as in VG-M	as in VG-M	k_{rl}: as in VG-M
VG-EPL	$\alpha = 2.4 \times 10^{-4}$ 1/Pa $n_v = 1.864$ $m_v = 0.464$ $S_{i0} = 0.4438$	$N_{l-EPL} = 3.2$ $k_{rl0-EPL} = 1.0$ $N_{g-EPL} = 2.6$ $k_{rg0-EPL} = 0.3948$ $S_{i0} = 0.4438$	$\alpha = 2.9 \times 10^{-4}$ 1/Pa $n_v = 2.266$ $m_v = 0.559$ $S_{i0} = 0.3894$	$N_{l-EPL} = 4.6$ $k_{rl0-EPL} = 1.0$ $N_{g-EPL} = 3.0$ $k_{rg0-EPL} = 0.3284$ $S_{i0} = 0.3894$
BC-vC	same as BC-B	$N_{l-vC} = 6.0$ $N_{g-vC} = 5.0$ $k_{rg0-vC} = 0.95$ $S_{li} = 0.11$	same as BC-B	$N_{l-vC} = 8.0$ $N_{g-vC} = 2.0$ $k_{rg0-vC} = 0.95$ $S_{li} = 0.05$

Table 3. Continued.

	Tuscaloosa		Mt. Simon	
Model	$S - P_c$	$k_r - S$	$S - P_c$	$k_r - S$
VG-M	$\alpha = 7.4 \times 10^{-4}$ 1/Pa $n_v = 1.669$ $m_v = 0.401$ $S_{li} = 0.05$	$m_v = 0.401$	$\alpha = 1.4 \times 10^{-4}$ 1/Pa $n_v = 1.669$ $m_v = 0.401$ $S_{li} = 0.22$	$m_v = 0.401$
BC-B	$P_e = 8.6 \times 10^2$ Pa $\lambda = 0.55$ $S_{li} = 0.05$	$\lambda = 0.55$	$P_e = 4.6 \times 10^3$ Pa $\lambda = 0.55$ $S_{li} = 0.22$	$\lambda = 0.55$
VG-C	as in VG-M		as in VG-M	
VG -hMC	as in VG-M	k_{rl}: as in VG-M	as in VG-M	k_{rl}: as in VG-M
VG-EPL	$\alpha = 7.4 \times 10^{-4}$ 1/Pa $n_v = 1.669$ $m_v = 0.401$ $S_{i0} = 0.7030$	$N_{l-EPL} = 4.7$ $k_{rl0-EPL} = 1.0$ $N_{g-EPL} = 3.2$ $k_{rg0-EPL} = 0.0767$ $S_{i0} = 0.7030$	$\alpha = 1.4 \times 10^{-4}$ 1/Pa $n_v = 1.669$ $m_v = 0.401$ $S_{i0} = 0.4371$	$N_{l-EPL} = 6.0$ $k_{rl0-EPL} = 1.0$ $N_{g-EPL} = 1.6$ $k_{rg0-EPL} = 0.4929$ $S_{i0} = 0.4371$
BC-vC	as in BC-B	$N_{l-vC} = 17.0$ $N_{g-vC} = 4.0$ $k_{rg0-vC} = 0.95$ $S_{li} = 0.05$	as in BC-B	$N_{l-vC} = 9.0$ $N_{g-vC} = 4.0$ $k_{rg0-vC} = 0.95$ $S_{li} = 0.22$

Table 4. Webb (2000) matching point saturations and capillary pressures for the Van Genuchten, Brooks-Corey, and Van Genuchten-Endpoint Power Law (VG-EPL) $S - P_c$ relations.

	Matching Point Saturation (-)	**Matching Point Capillary Pressure (Pa)**
Berea		
Van Genuchten	0.129	3.61×10^5
Brooks-Corey	0.137	4.79×10^5
Van Genuchten – EPL	0.504	5.46×10^5
Paaratte		
Van Genuchten	0.055	2.12×10^5
Brooks-Corey	0.058	4.14×10^5
Van Genuchten – EPL	0.422	3.48×10^4
Tuscaloosa		
Van Genuchten	0.063	7.99×10^5
Brooks-Corey	0.068	1.13×10^6
Van Genuchten – EPL	0.812	5.68×10^3
Mt. Simon		
Van Genuchten	0.271	4.07×10^5
Brooks-Corey	0.287	4.09×10^5
Van Genuchten – EPL	0.524	1.15×10^5

Table 5. Input parameters for the 1-D and 2-D test cases (after Mathias et al. 2013)

Parameter	**Value**
Well radius	0.2 m
Radial extent	20 km
Initial pressure	10 MPa
Temperature	40^{o} C
Salt mass fraction	0
Formation thickness	30 m
Injection duration	30 years
Injection rate	15 kg/s

Figures

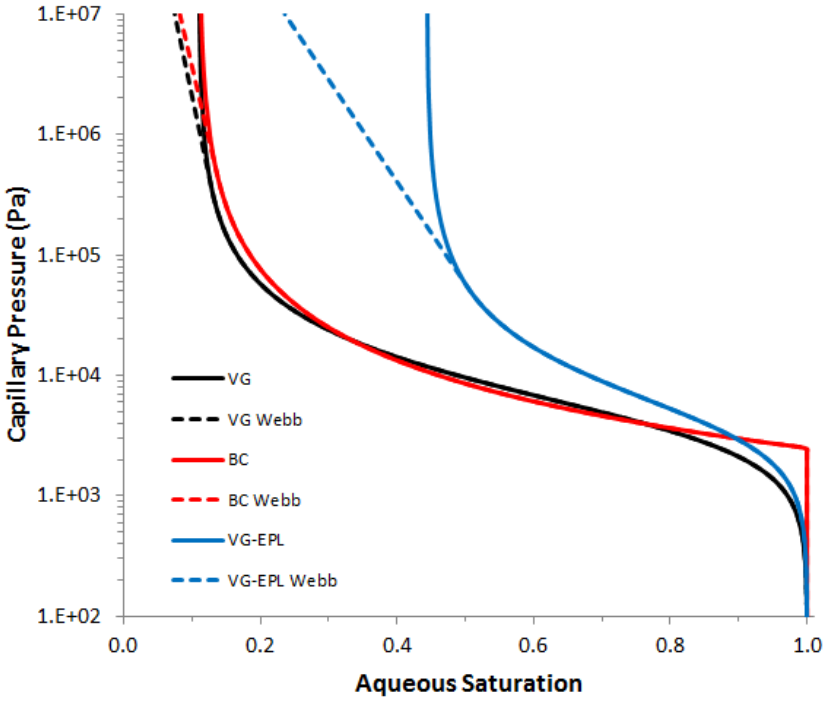

(a)

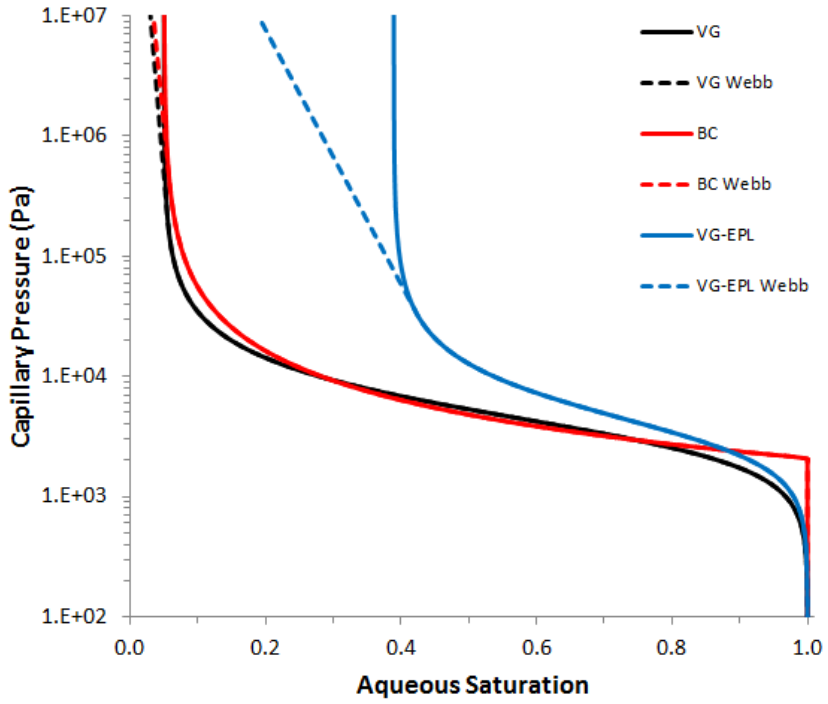

(b)

Figure 1. Capillary pressure-saturation relations, with and without the Webb (2000) extension, for (a) Berea, (b) Paaratte, (c) Tuscaloosa, and (4) Mt.Simon sandstone.

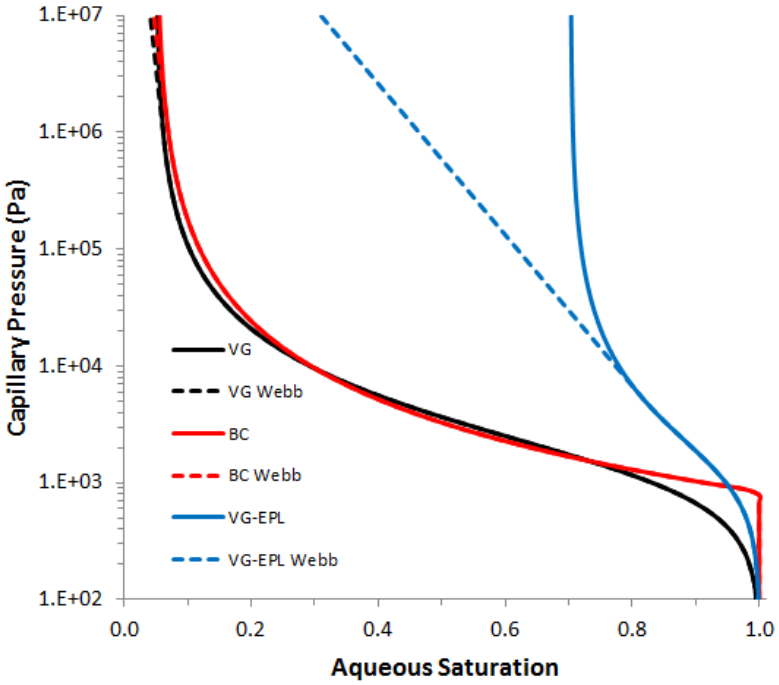

(c)

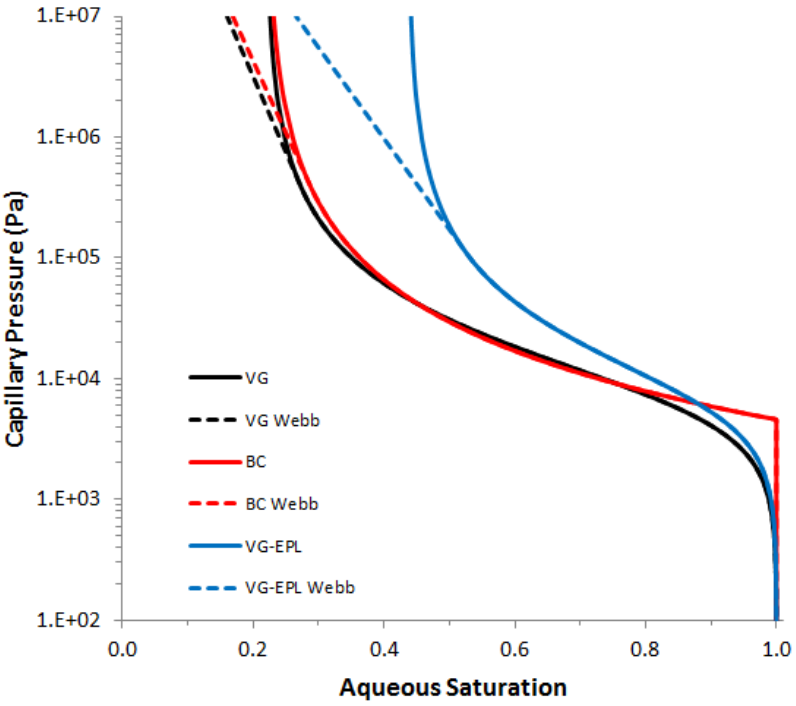

(d)

Figure 1. Continued.

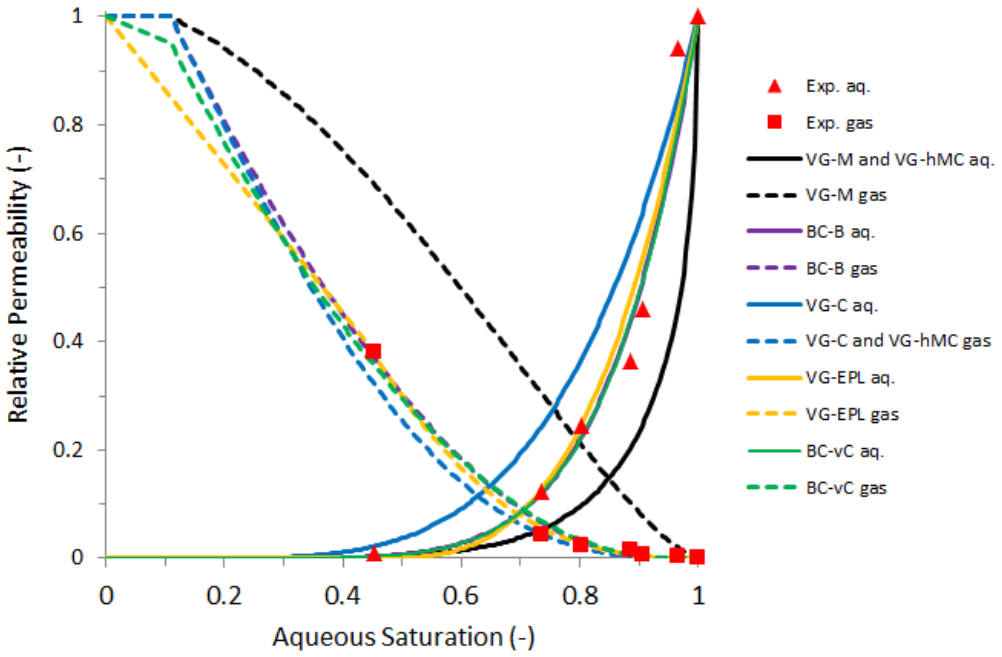

(a)

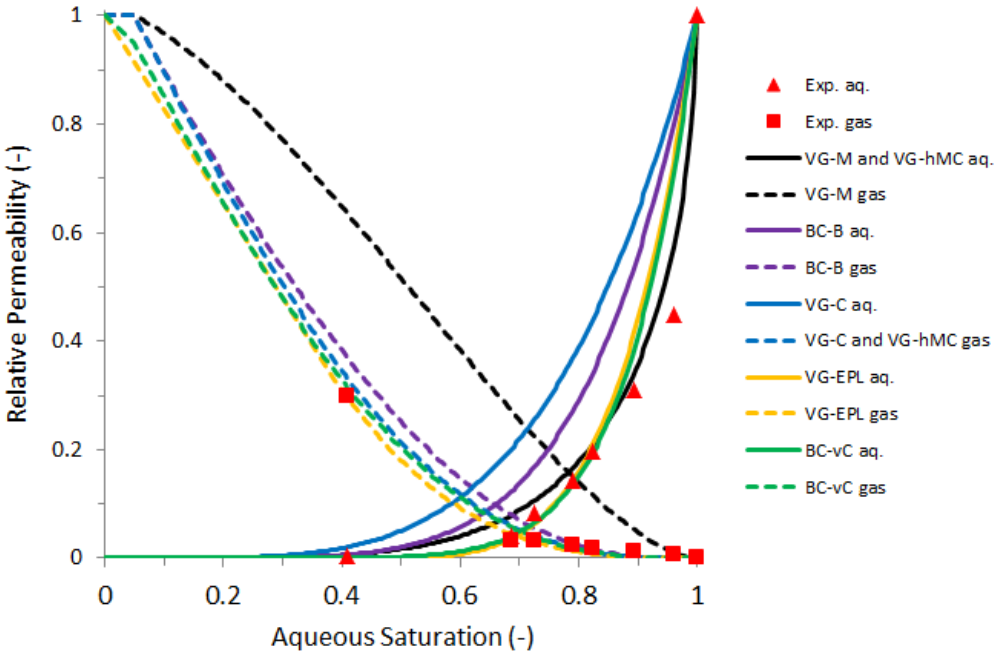

(b)

Figure 2. Experimental (from Krevor et al., 2012) and model relative permeabilities for (a) Berea, (b) Paaratte, (c) Tuscaloosa, and (d) Mt. Simon sandstone.

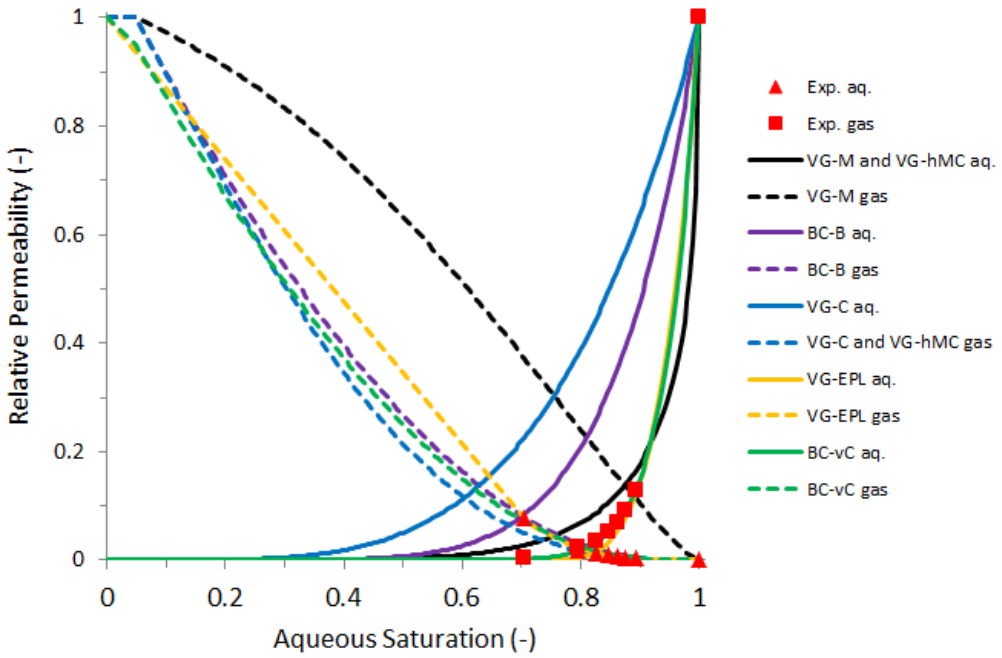

(c)

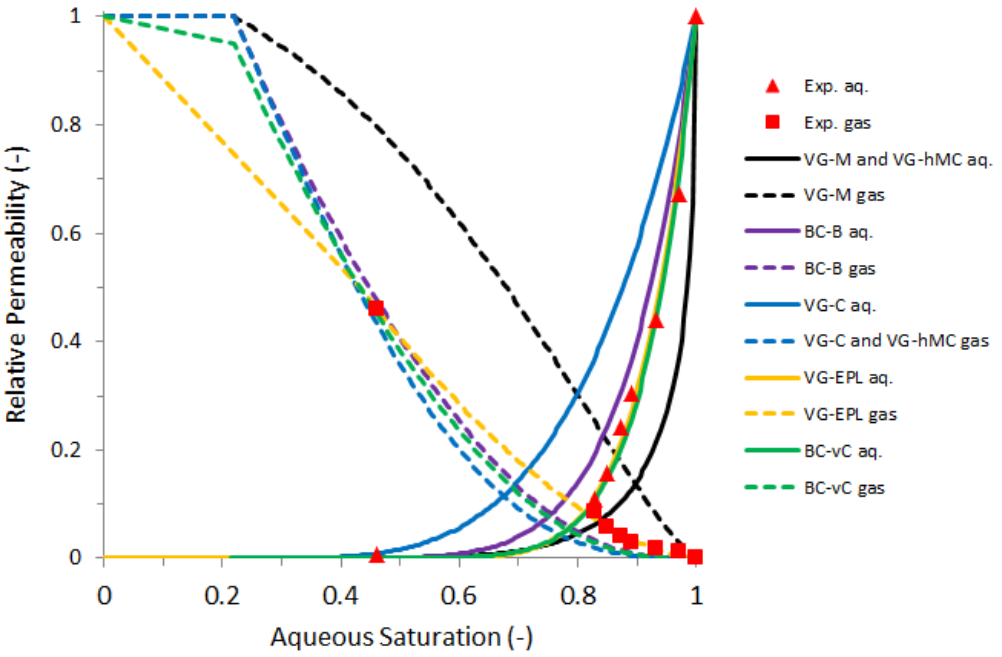

(d)

Figure 2. Continued.

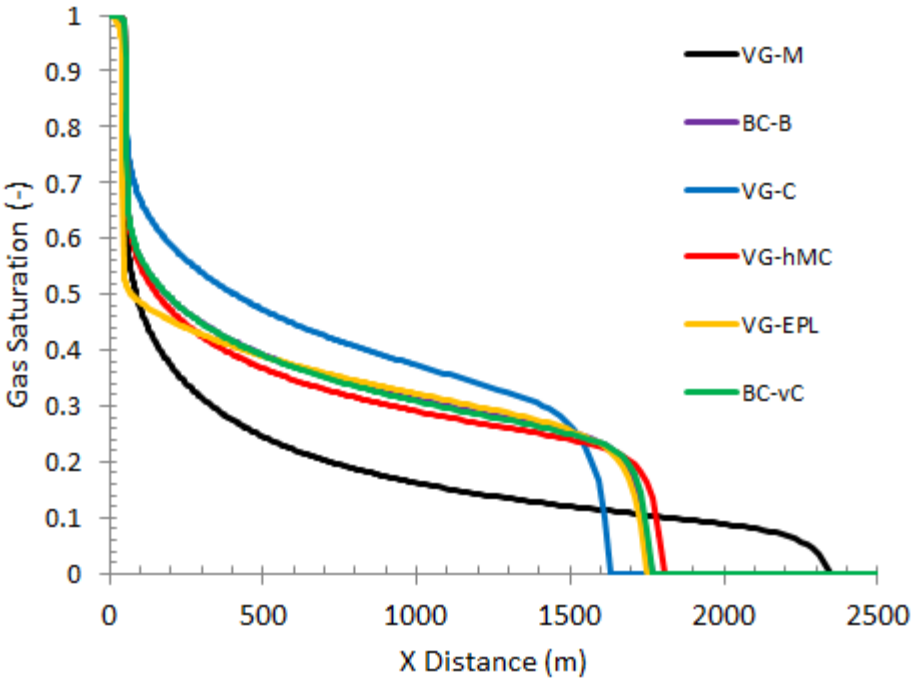

(a)

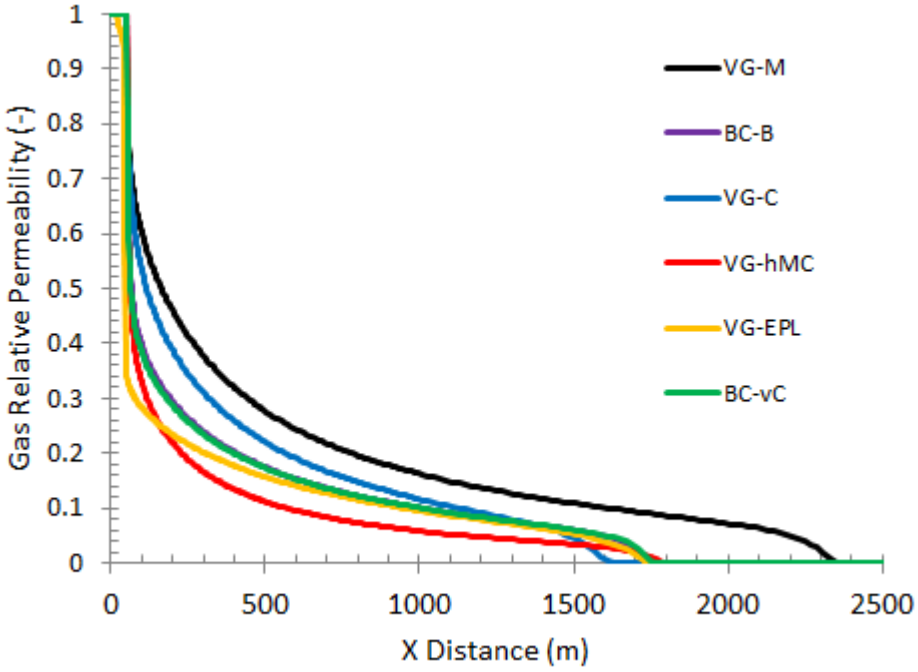

(b)

Figure 3. (a) Gas saturation, (b) gas relative permeability, and (c) well pressure at the end of the injection period for the 1-D Berea simulations.

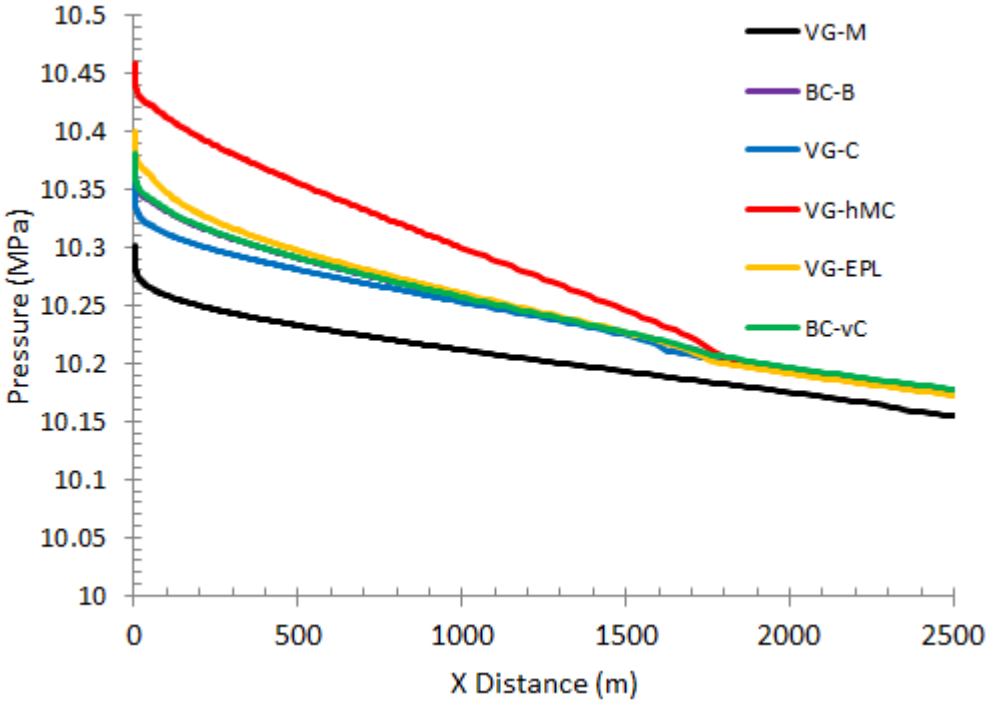

(c)

Figure 3. Continued.

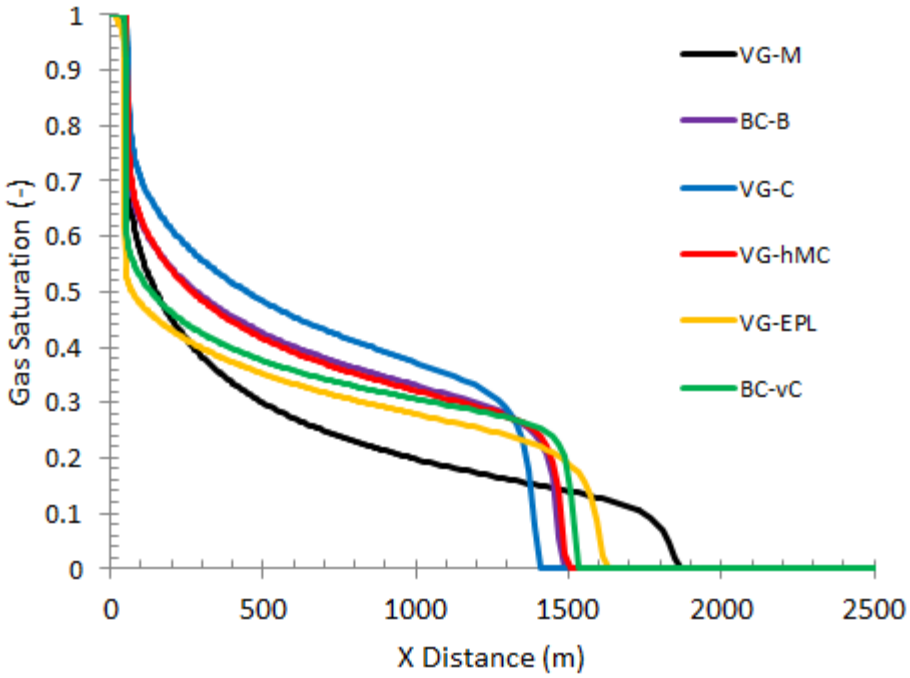

(a)

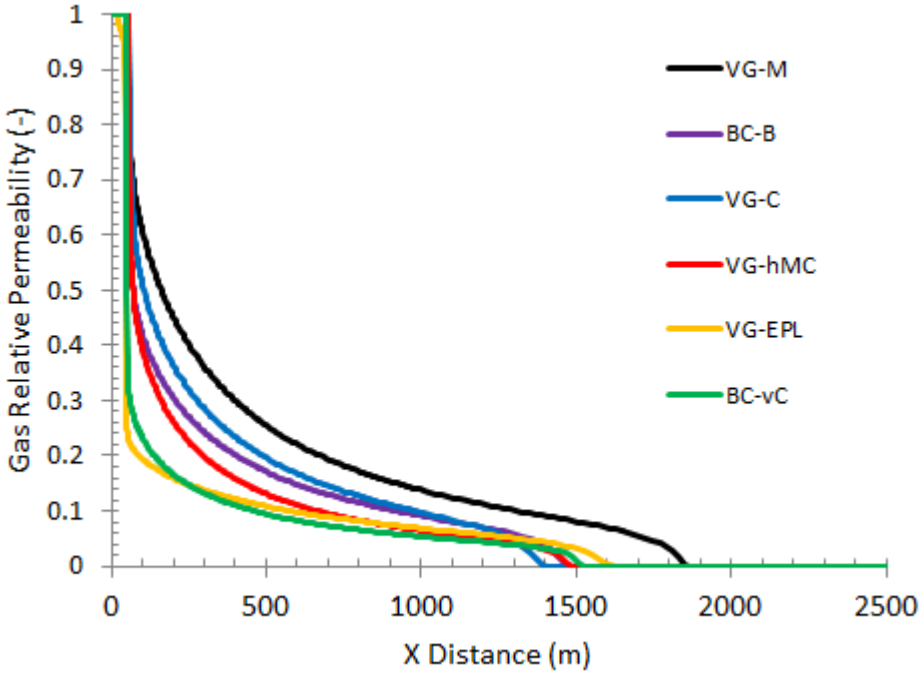

(b)

Figure 4. (a) Gas saturation, (b) gas relative permeability, and (c) well pressure at the end of the injection period for the 1-D Paaratte simulations.

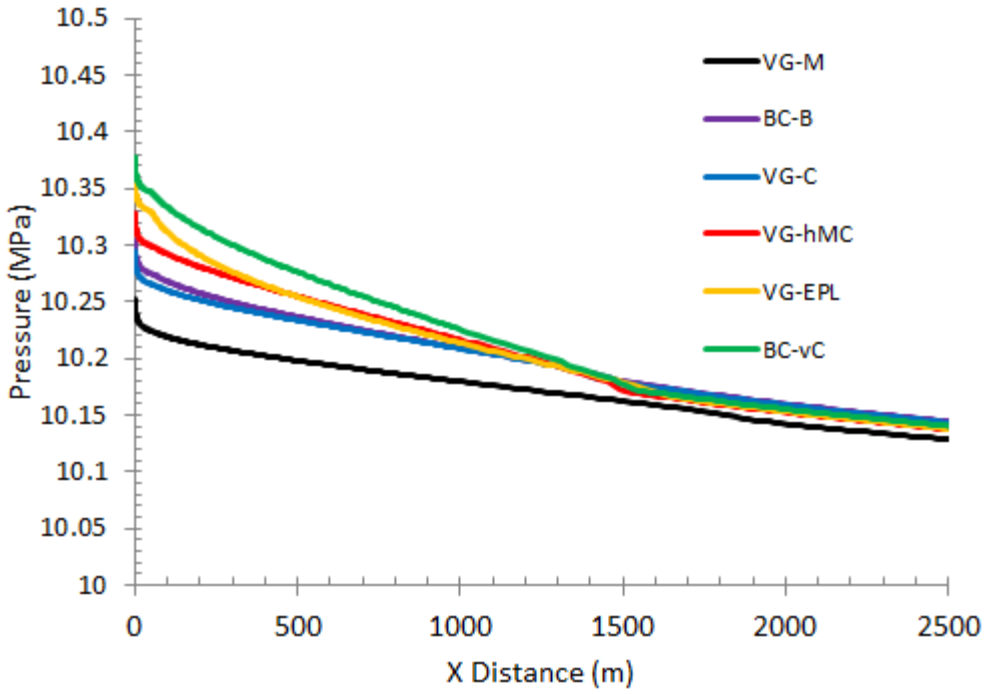

(c)

Figure 4. Continued.

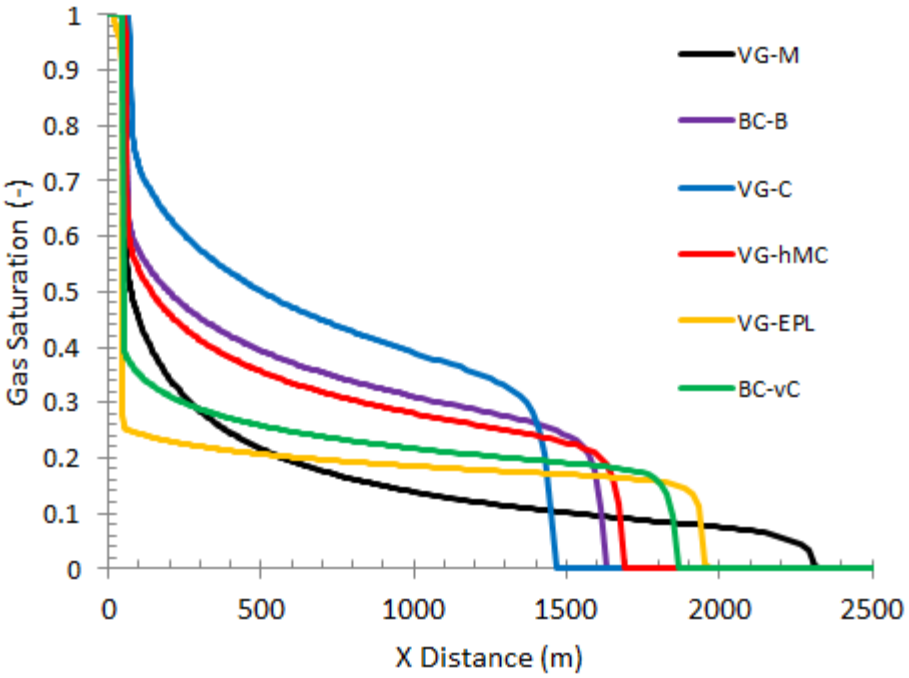

(a)

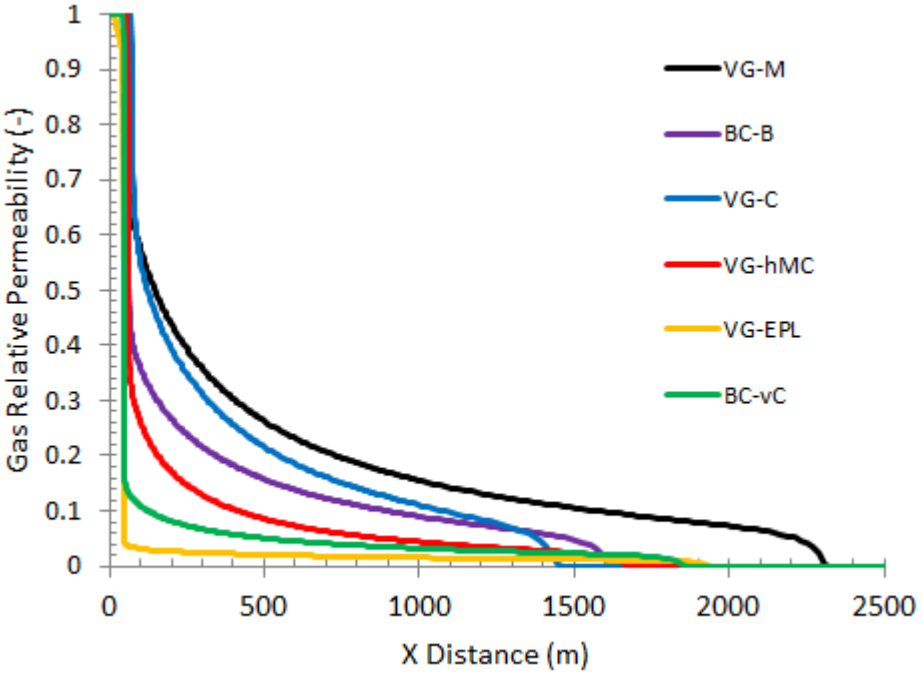

(b)

Figure 5. (a) Gas saturation, (b) gas relative permeability, and (c) well pressure at the end of the injection period for the 1-D Tuscaloosa simulations.

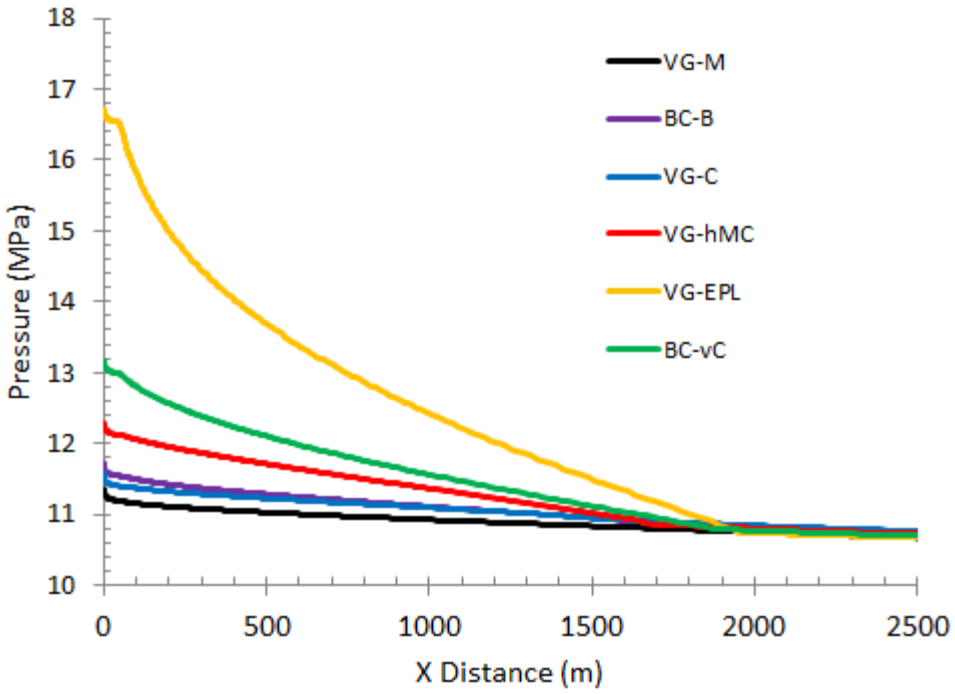

(c)

Figure 5. Continued.

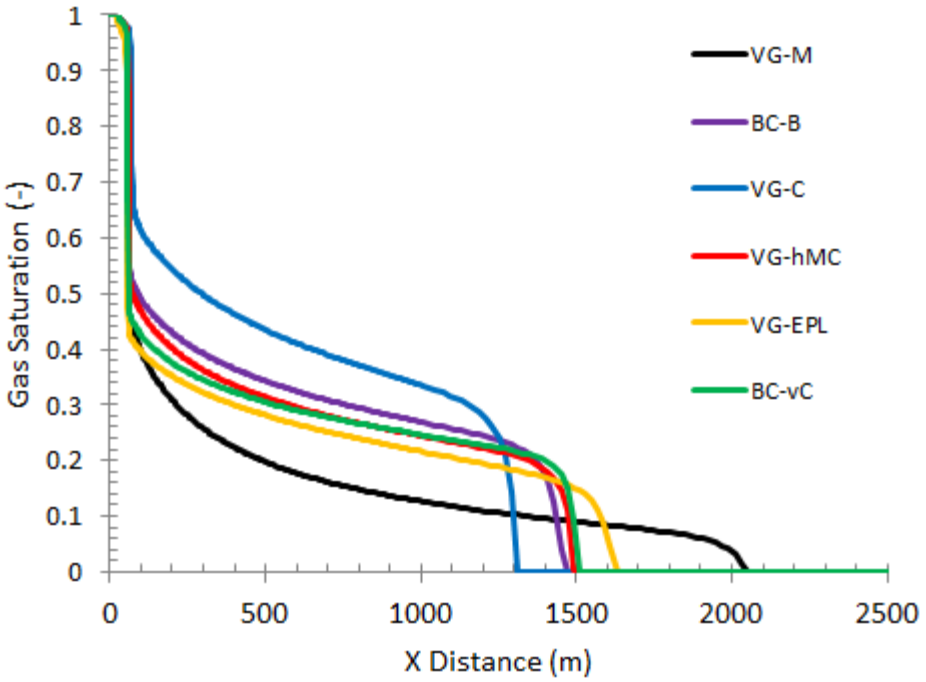

(a)

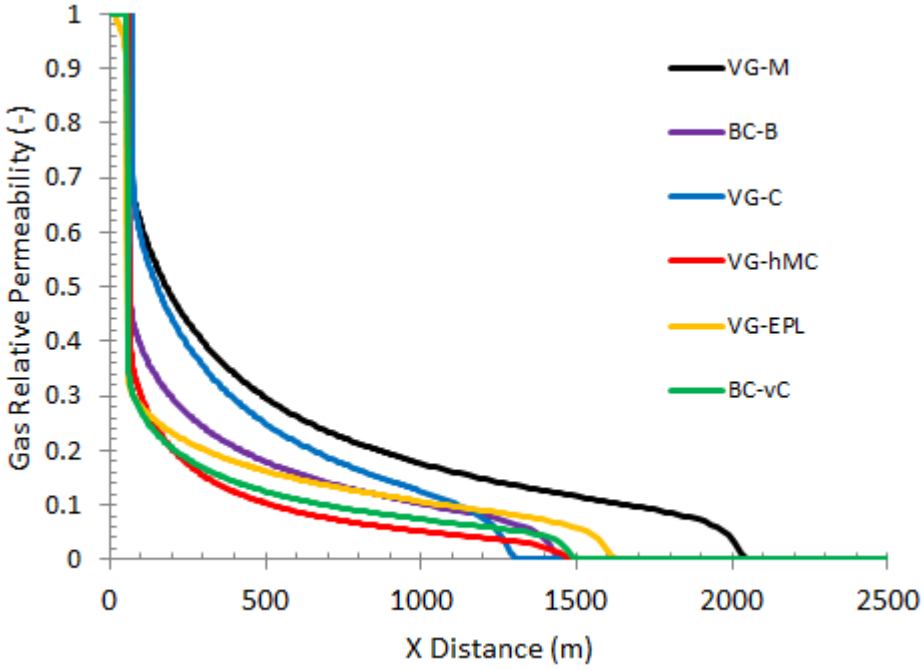

(b)

Figure 6. (a) Gas saturation, (b) gas relative permeability, and (c) well pressure at the end of the injection period for the 1-D Mt. Simon simulations.

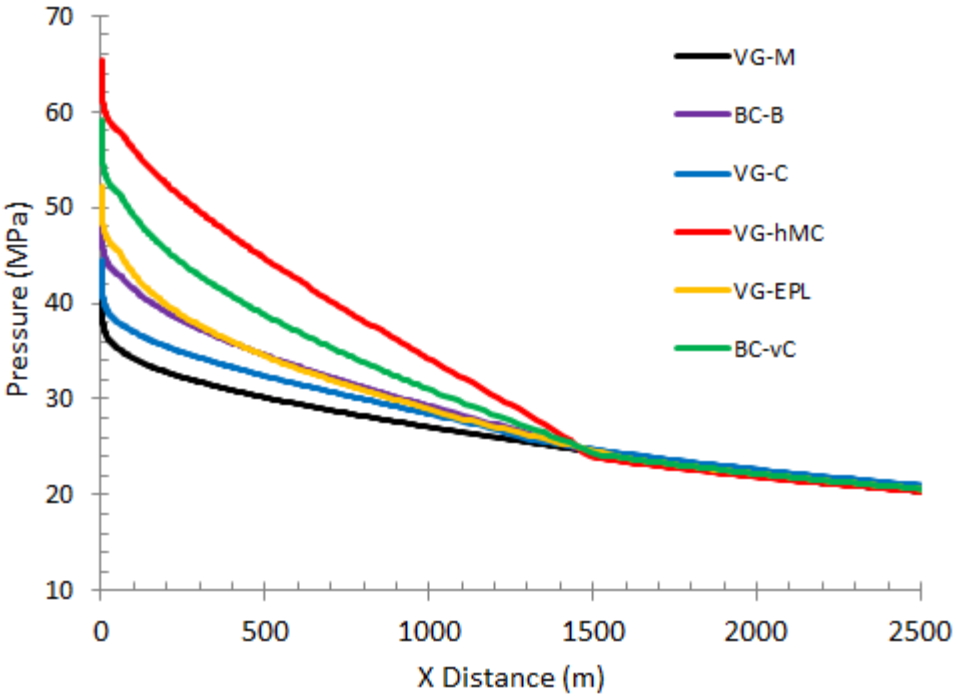

(c)

Figure 6. Continued.

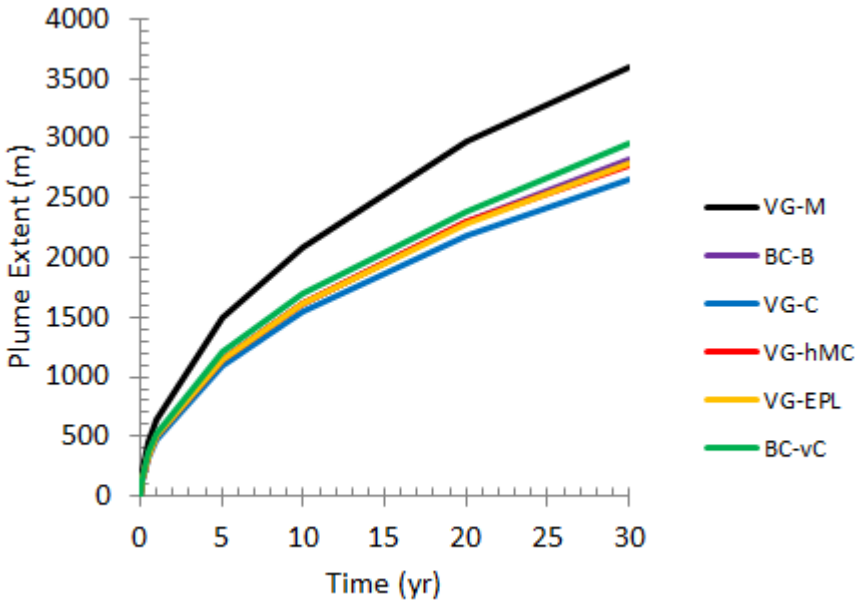

(a)

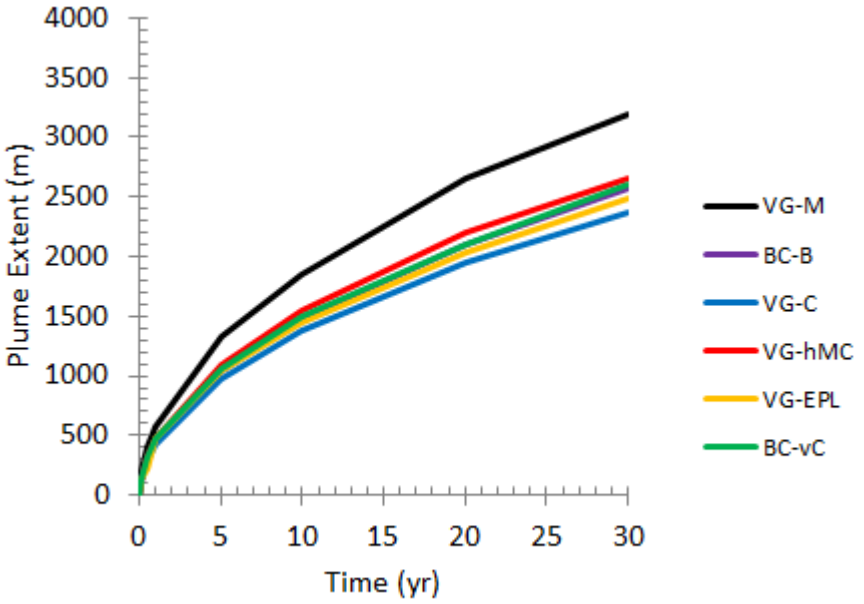

(b)

Figure 7. Plume extent (horizontal distance from injection well) over time for 2-D simulation of injection into (a) Berea, (b) Paaratte, (c) Tuscaloosa, and (d) Mt. Simon sandstone.

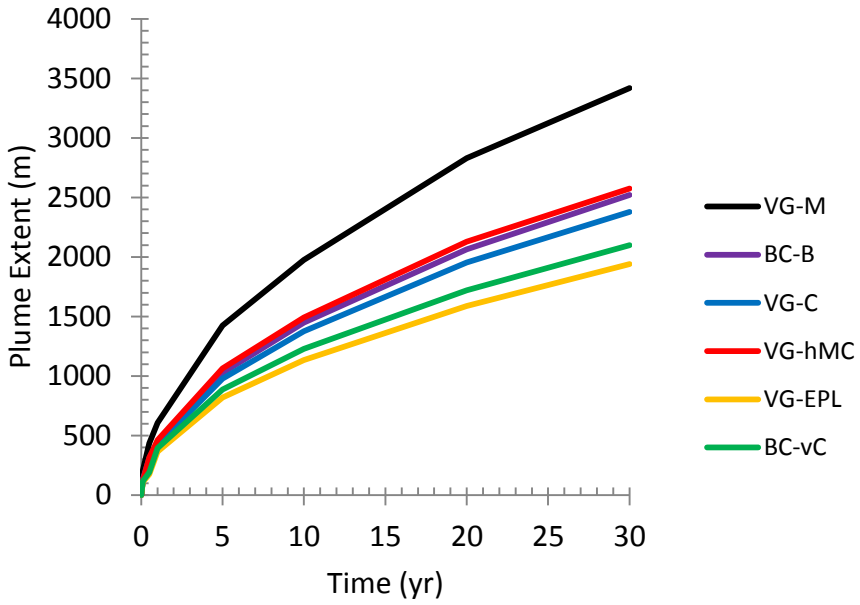

(c)

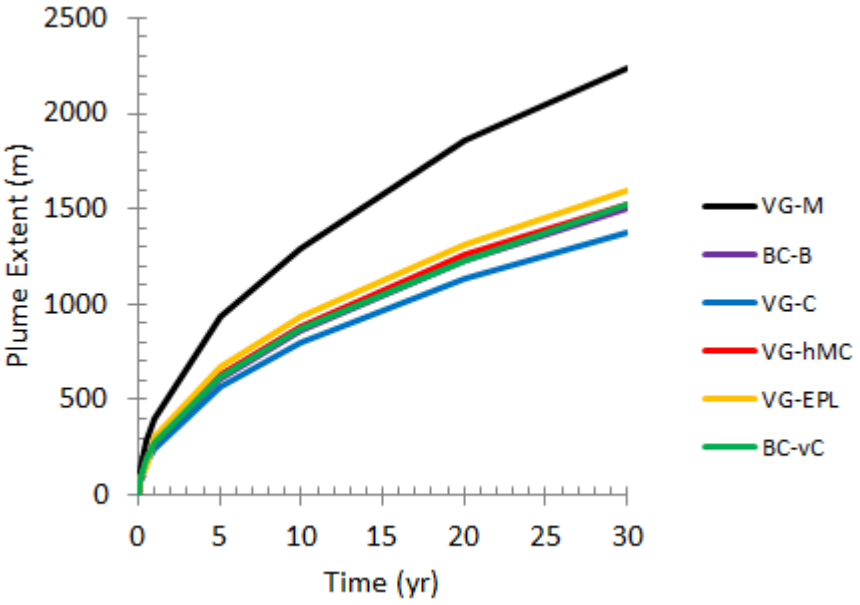

(d)

Figure 7. Continued.

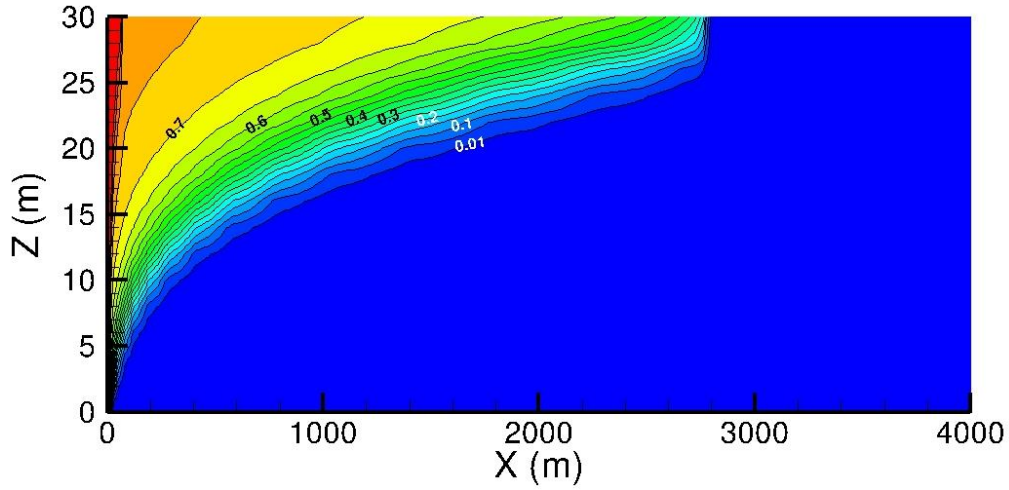

(a)

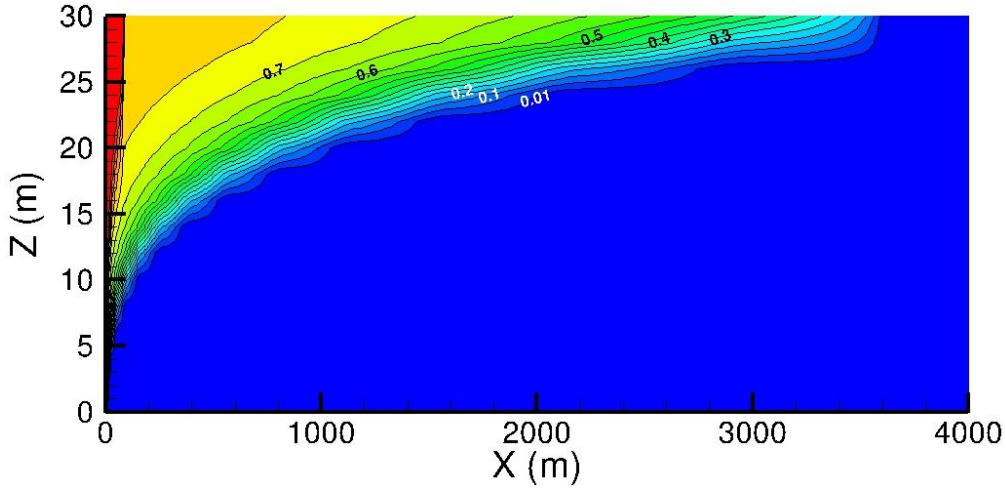

(b)

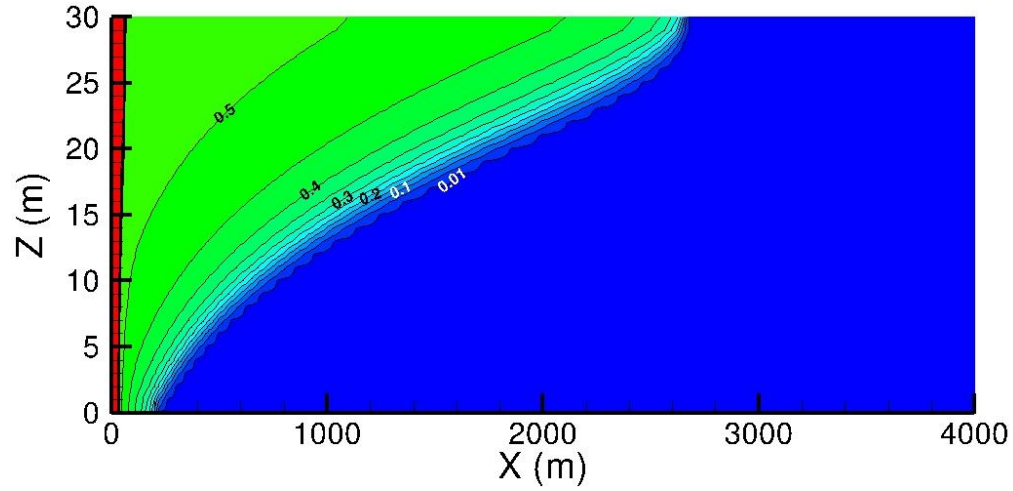

(c)

Figure 8. Gas saturation after 30 years of injection into Berea sandstone using the (a) BC-vC, (b) VG-M, and (c) VG-EPL $k_r - S - P_c$ model.

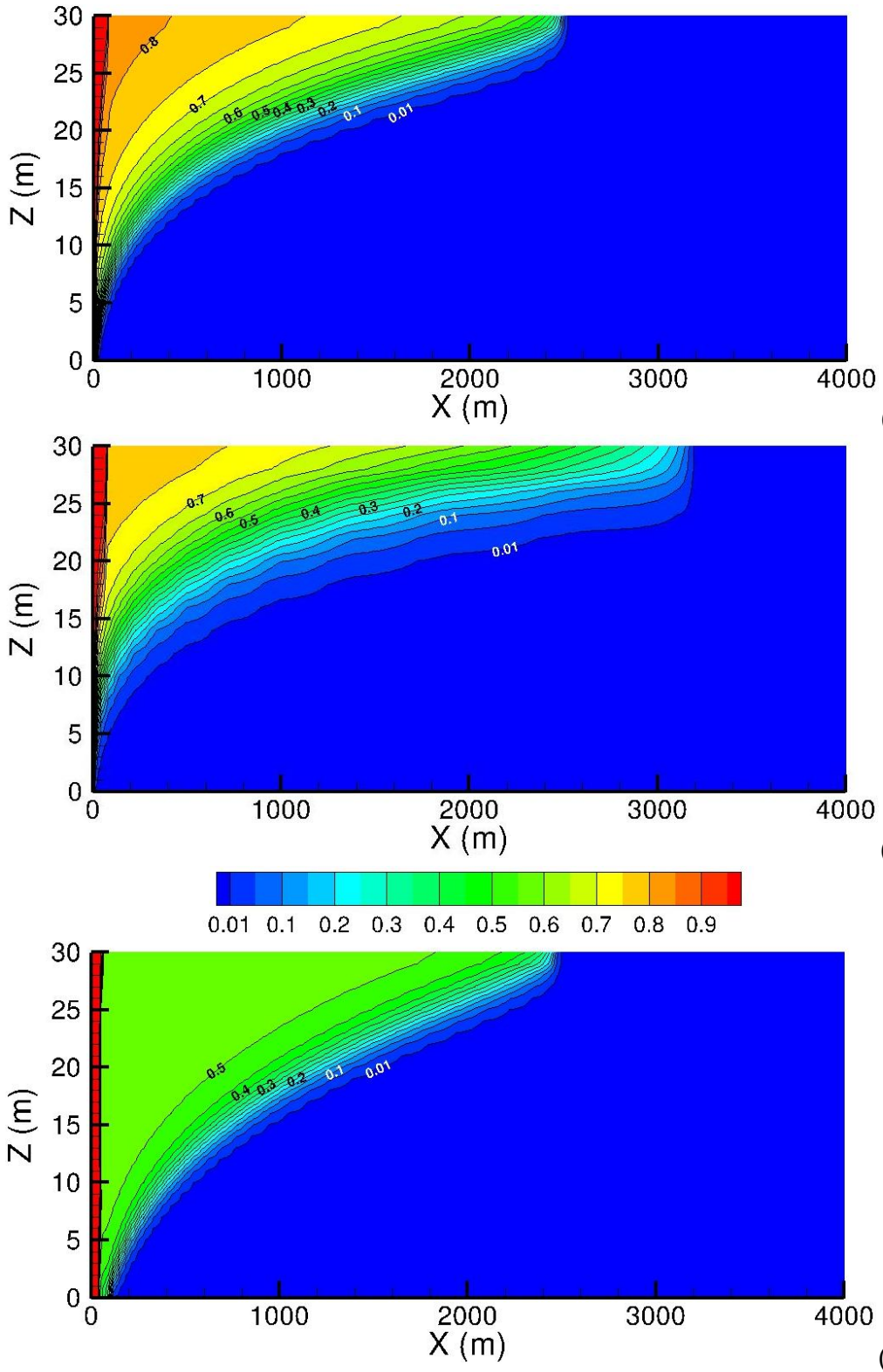

Figure 9. Gas saturation after 30 years of injection into Paaratte sandstone using the (a) BC-vC, (b) VG-M, and (c) VG-EPL $k_r - S - P_c$ model.

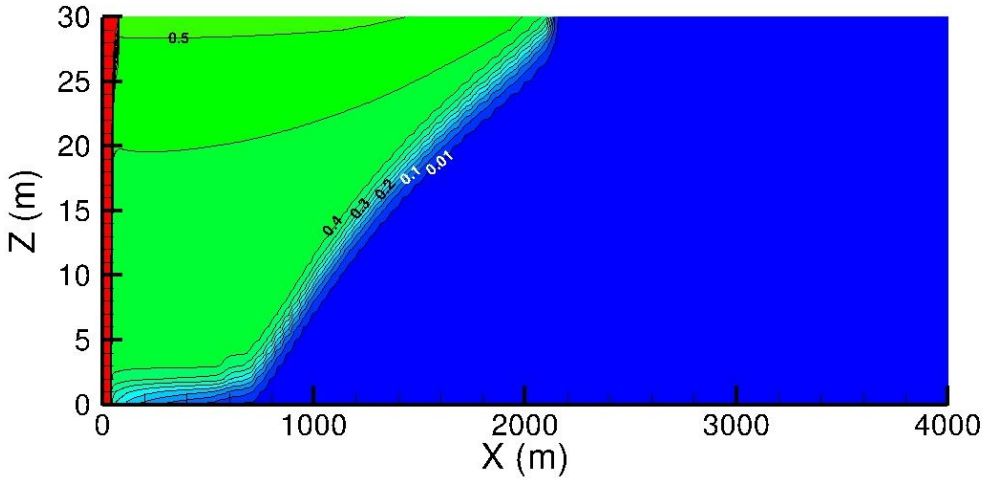

(a)

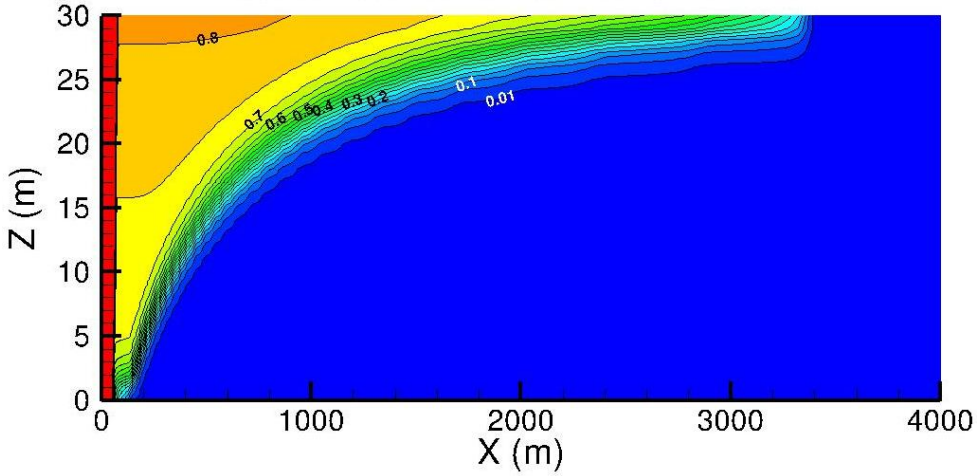

(b)

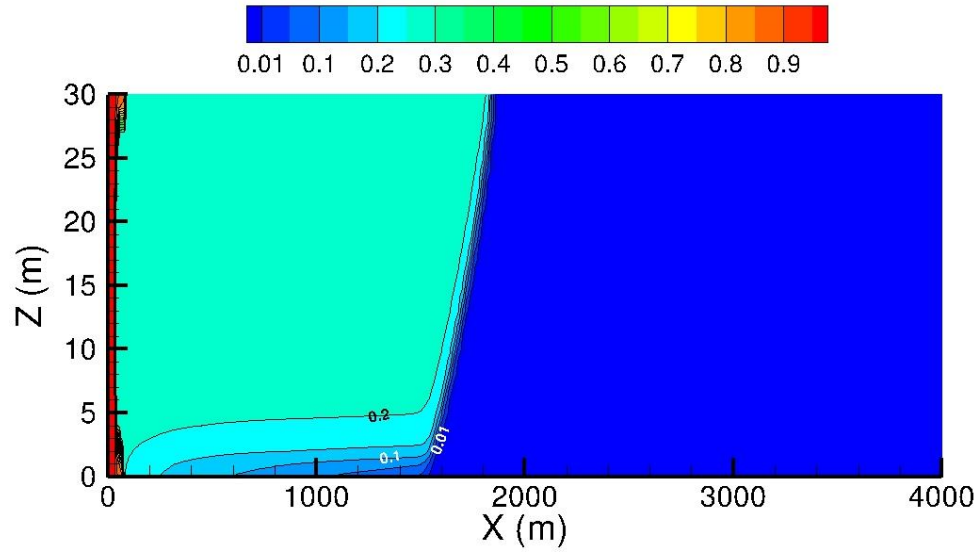

(c)

Figure 10. Gas saturation after 30 years of injection into Tuscaloosa sandstone using the (a) BC-vC, (b) VG-M, and (c) VG-EPL $k_r - S - P_c$ model.

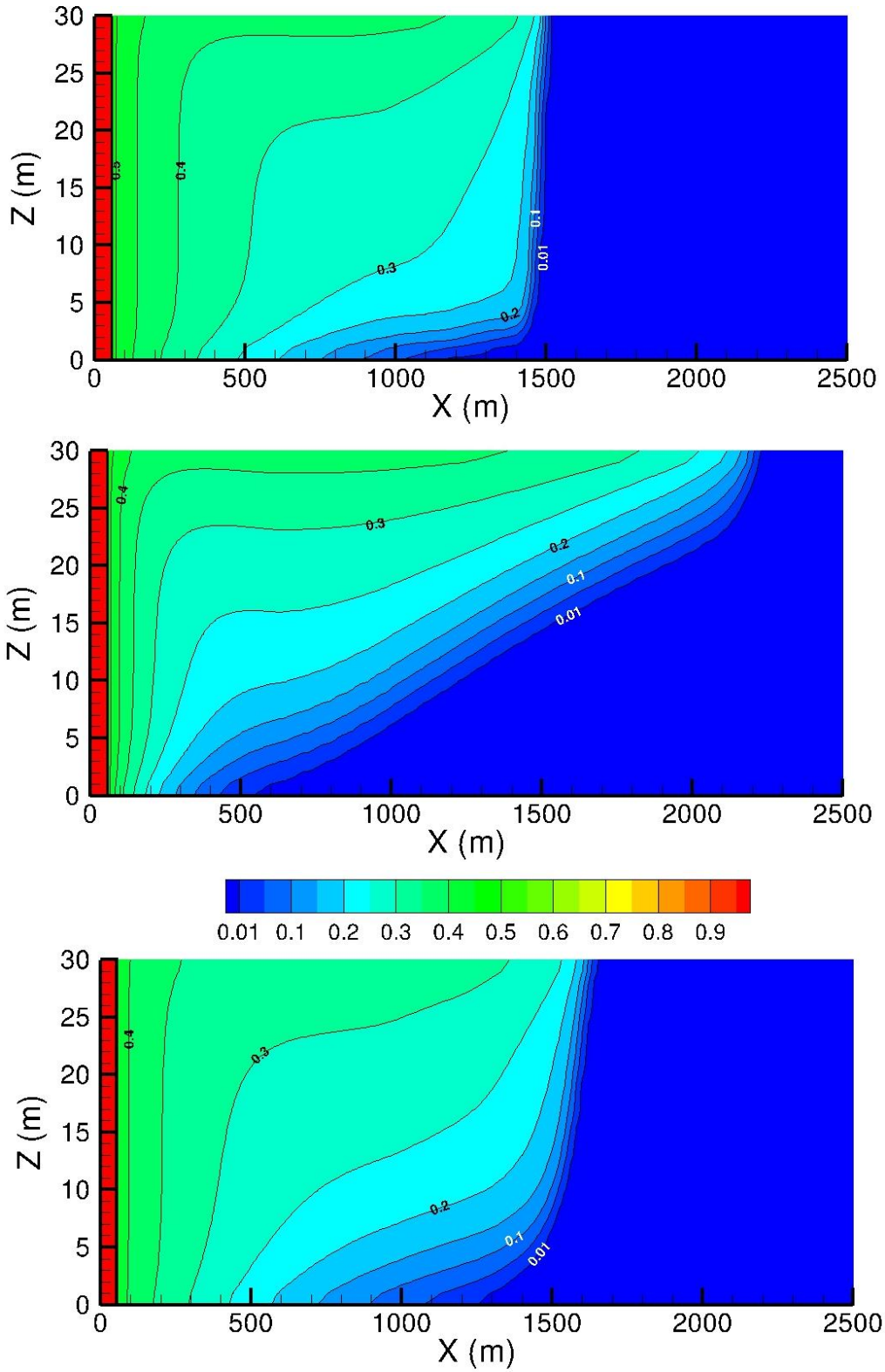

Figure 11. Gas saturation after 30 years of injection into Mt. Simon sandstone using the (a) BC-vC, (b) VG-M, and (c) VG-EPL $k_r - S - P_c$ model.

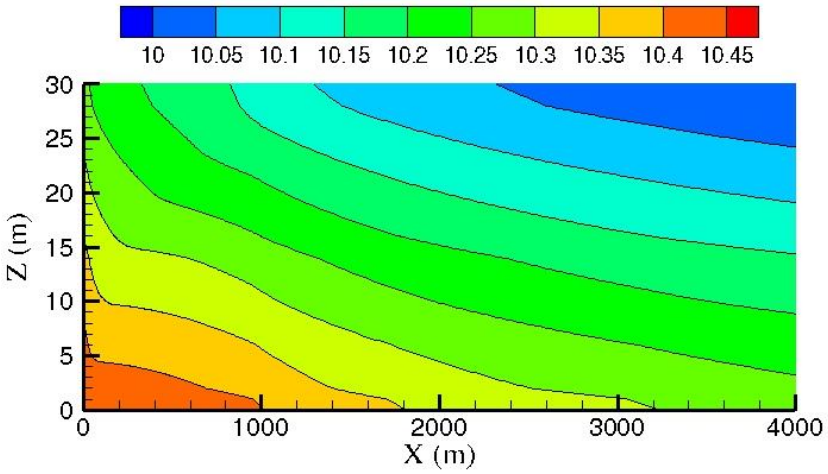

Figure 12. Formation fluid pressures (in MPa) at the end of the injection period for the Berea BC-vC simulation.

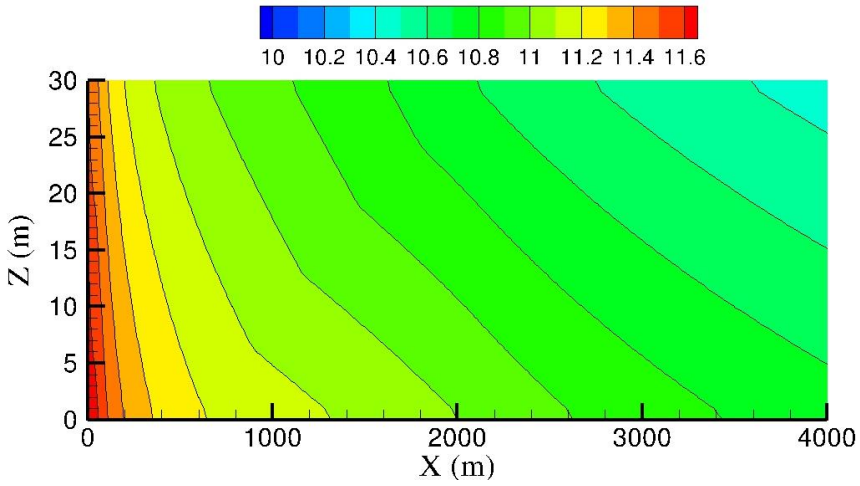

(a)

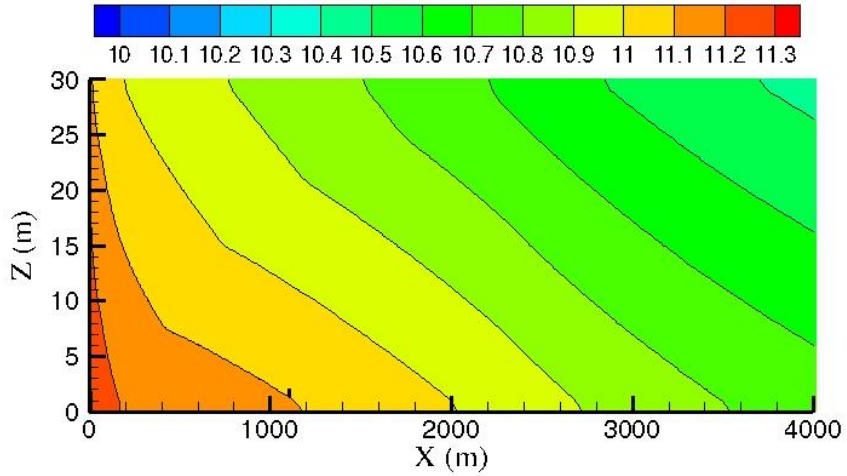

(b)

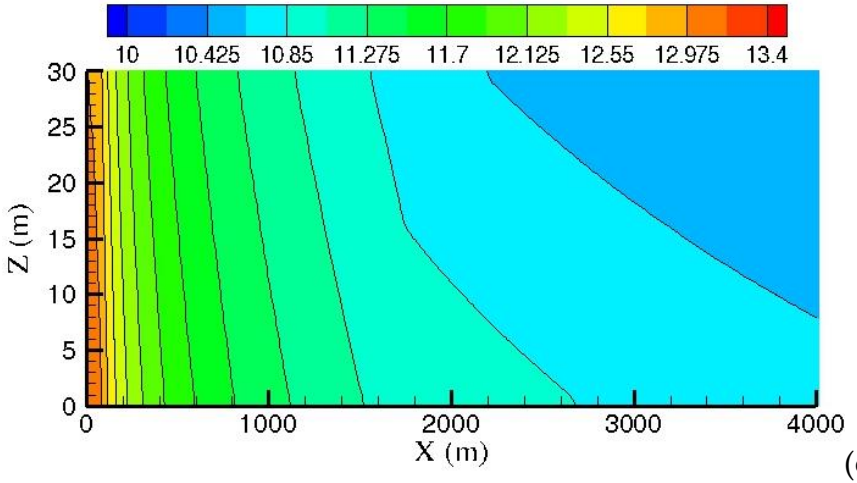

(c)

Figure 13. Formation pressure distribution (in MPa) at the end of the injection period for the Tuscaloosa (a) BC-vC, (b) VG-hMC, and (c) VG-EPL simulations.

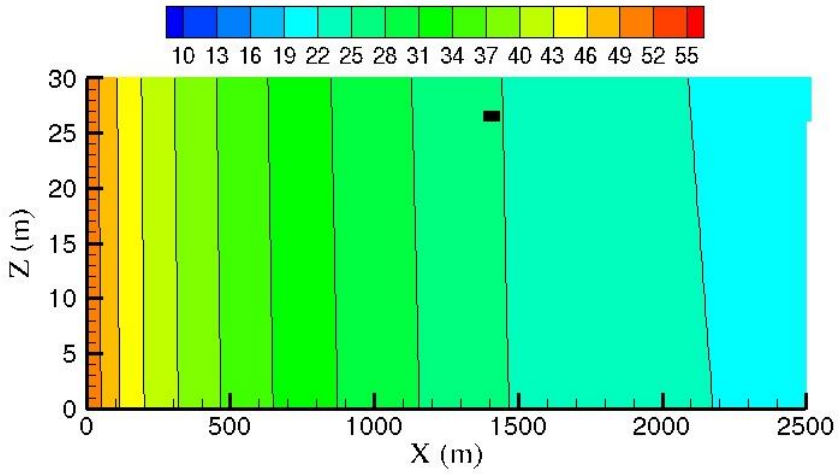

(a)

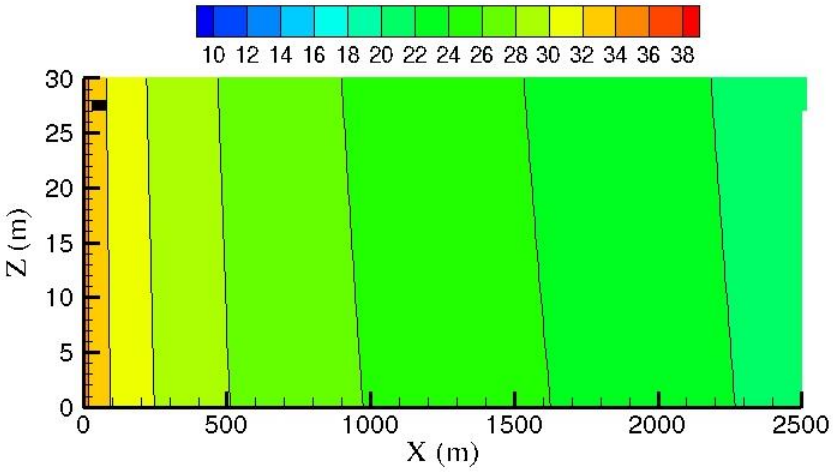

(b)

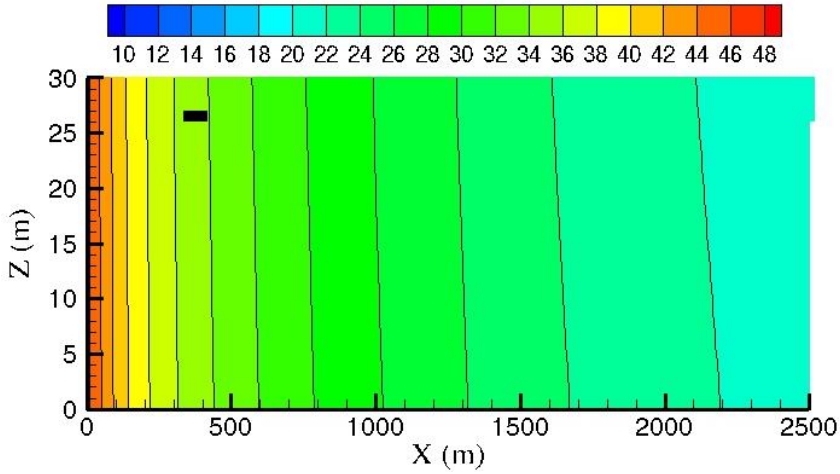

(c)

Figure 14. Formation pressure distribution (in MPa) at the end of the injection period for the Mt.Simon (a) BC-vC, (b) VG-hMC, and (c) VG-EPL simulations.

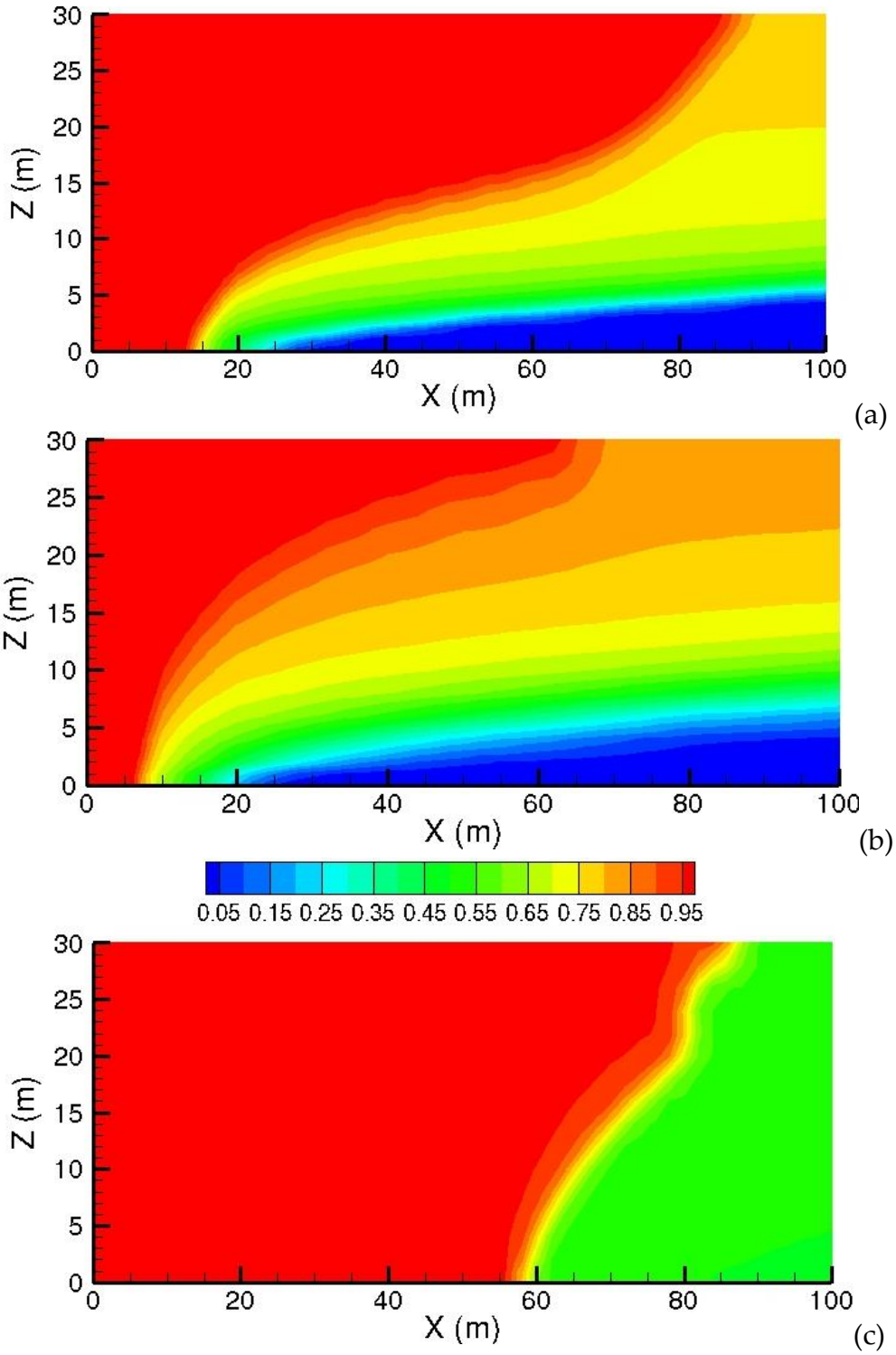

Figure 15. Near-well gas saturation at the end of the 30-yr injection period into Berea sandstone for the (a) VG-M, (b) VG-C, and (c) VG-EPL $k_r - S - P_c$ models.

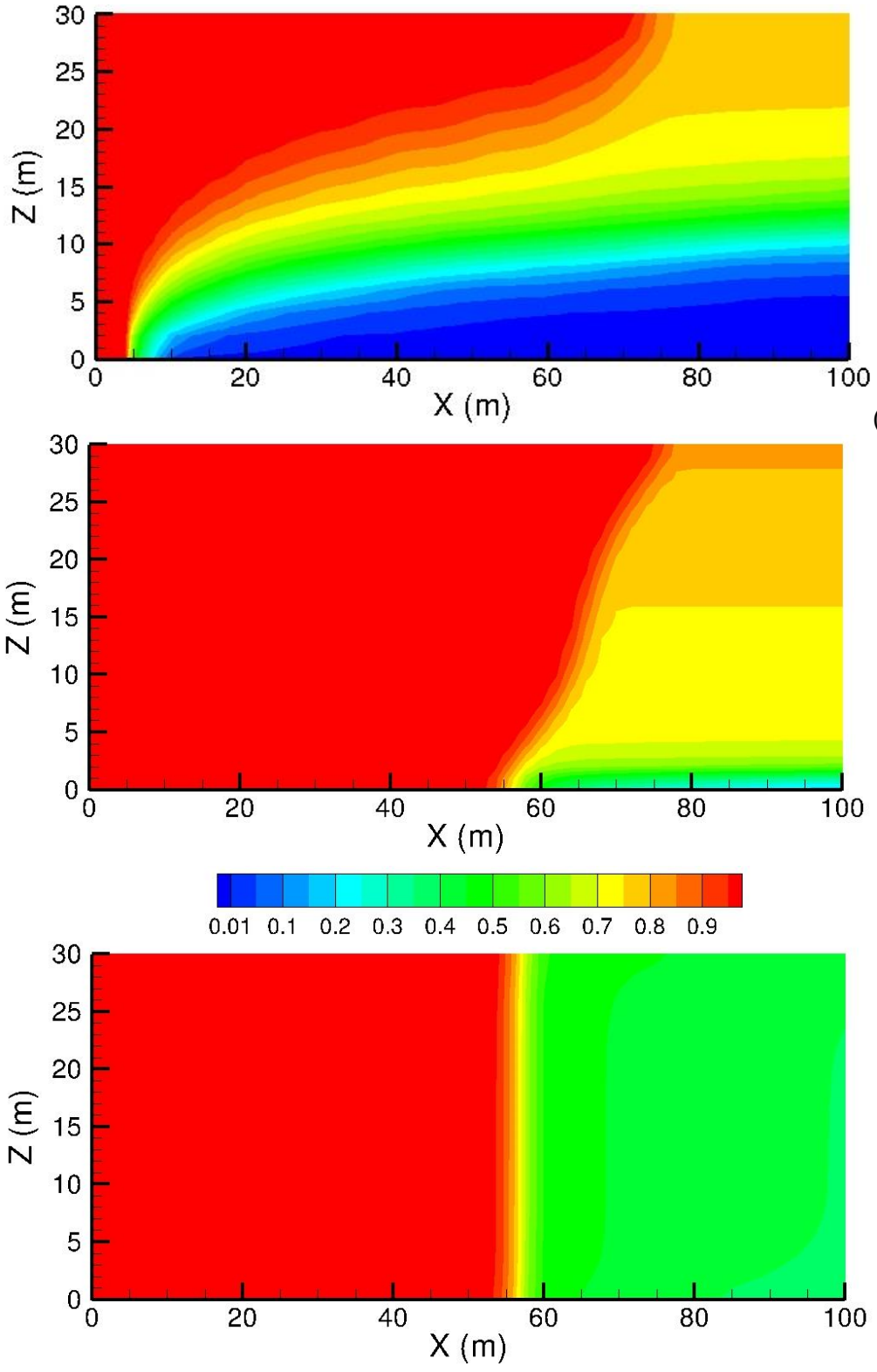

Figure 16. Near-well gas saturation at the end of the 30-yr injection period into (a) Paaratte, (b) Tuscaloosa, and (c) Mt. Simon sandstone for the VG-M $k_r - S - P_c$ model.